Lying in wait: deep and shallow evolution of dacite beneath Volcán de Santa María, Guatemala

B. S. SINGER[1]*, B. R. JICHA[1], J. H. FOURNELLE[1], B. L. BEARD[1], C. M. JOHNSON[1], K. E. SMITH[1], S. E. GREENE[1], N. T. KITA[1], J. W. VALLEY[1], M. J. SPICUZZA[1] & N. W. ROGERS[2]

[1]*Department of Geoscience, University of Wisconsin-Madison, Madison, USA*

[2]*Department of Earth and Environmental Science, The Open University, Milton Keynes, UK*

**Corresponding author (e-mail: bsinger@geology.wisc.edu)*

Abstract: The Plinian eruption in October 1902 of 8.5 km^3 of dacitic pumice and minor basaltic andesite scoria and ash at Volcán de Santa María, Guatemala violently interrupted a 25 kyr period of repose that had followed ~75 kyr of cone-growth via extrusion of 8 km^3 of basaltic andesite lava. Two-oxide and pyroxene thermometry reveal an oxidized (Ni-NiO + 2 log units) and thermally-zoned magma body in which basaltic andesite with 54 wt% SiO_2 at 1020 °C and dacite with 65 wt% SiO_2 at 870 °C coexisted. Plagioclase in dacite pumice and basaltic andesite scoria shows remarkably similar zoning characterized by repeated excursions toward high anorthite and increases in Mg, Fe, and Sr associated with resorption surfaces along which dacitic to rhyolitic melt inclusions are trapped. The melt inclusions increase slightly in K_2O as SiO_2 increases from 69 to 77 wt%, whereas H_2O contents between 5.2 and 1.4 wt% drop with increasing K_2O. These observations suggest that crystallization of the plagioclase, and evolution of a high-silica rhyolitic residual melt, occurred mainly in the conduit as the compositionally-zoned magma body decompressed and degassed from >180 MPa, or >5 km depth, toward the surface. The similarity of plagioclase composition, zoning, and melt inclusion compositions in pumice and scoria suggests that crystals which grew initially in the cooler dacite, were exchanged between dacitic and basaltic andesite magma as the two magmas mingled and partially mixed *en route* to the surface. Since 1922 > 1 km^3 of dacitic magma similar to the 1902 pumice has erupted effusively to form the Santiaguito dome complex in the 1902 eruption crater.

Trace element and Sr–Nd–Pb–O and U–Th isotope data indicate that cone-forming basaltic andesite lavas record processes operating in the deep crust in which wallrock heating sufficient to induce partial melting and assimilation involved several pulses of recharging mantle-derived basalt over at least 50 kyr. A fundamental shift in process coincides with the termination of cone-building at 25 ka: the 1902 dacite reflects >40% fractional crystallization of plagioclase + amphibole + clinopyroxene + magnetite from ~20 km^3 of basaltic andesite magma left-over following cone-building that cooled slowly without assimilating additional crust. Small contrasts in Sr–Nd–Pb ratios, a modest contrast in $\delta^{18}O$(WR), and a large difference in the ($^{238}U/^{230}Th$) activity ratio between the 1902 scoria and dacite indicate that these two magmas are not consanguineous, rather this basaltic andesite is likely a recent arrival in the system. A glass–whole rock–magnetite–amphibole ^{238}U–^{230}Th isochron of 9.5 ± 2.5 ka for a 1972 Santiaguito dacite lava suggests that deeper, occluded portions of the silicic magma body, not erupted in 1902, incubated in the crust for at least 10 kyr prior to the 1902 eruption. Basaltic andesite inclusions in the Santiaguito dacite lava domes are interpreted to be modified remnants of the cone-forming magma parental to the 1902 dacite.

Supplementary material: Electron probe analyses of glass standards, and SIMS data from standards and melt inclusions for the hydrogen measurements are available at http://www.geolsoc.org.uk/SUP18606

The origin of andesitic to dacitic magma in subduction zones remains a major focus of igneous petrology owing to the central role it plays in crustal evolution and the hazards posed by explosive, often deadly, eruptions. Many eruptions of dacite also contain lesser amounts of more mafic components, basalt to basaltic andesite in composition, that beg the question of whether the dacite is genetically related to the mafic magma, or if the ascent of mafic magma into the dacite may have promoted eruption (e.g. Sparks *et al.* 1977; Pallister *et al.* 1992). Whereas geochemical observations (e.g. Hildreth & Moorbath 1988) and theoretical models (e.g. Dufek & Bergantz 2005; Annen *et al.* 2006) provide a conceptual framework for understanding how intermediate magmas result from the

From: Gómez-Tuena, A., Straub, S. M. & Zellmer, G. F. (eds) 2014. *Orogenic Andesites and Crustal Growth*. Geological Society, London, Special Publications, **385**, 209–234.
First published online June 11, 2013, http://dx.doi.org/10.1144/SP385.2

interaction of hydrous mantle-derived basalt with lower crustal rocks that partially melt and thus blend with the basalt, many details of the processes involved, including their timescales, remain obscure. Recent advances in $^{40}Ar/^{39}Ar$ geochronology have made it possible to date precisely latest Pleistocene and Holocene volcanic rocks in subduction zones (e.g. Jicha & Singer 2006; Hora *et al.* 2007; Jicha *et al.* 2012). In turn, this makes several tens of thousands of years of pre-historic eruptions amenable to U-series isotope disequilibrium study, thereby linking volcano growth episodes, large explosive eruptions, or collapse events with specific magmatic processes (e.g. Jicha *et al.* 2005, 2007, 2009; Hora *et al.* 2009). Moreover, the resulting estimates for the timing of mixing or recharge events, and duration of crystallization/pluton formation or partial melting episodes provide unique insights on the dynamics of intermediate magma formation (e.g. Hawkesworth *et al.* 2000; Bacon & Lowenstern 2005; Jicha *et al.* 2005; Bacon *et al.* 2007). In this light, $^{40}Ar/^{39}Ar$ dating (Escobar-Wolf *et al.* 2010; Singer *et al.* 2011) and U-series isotope (Jicha *et al.* 2010) studies of pre-historic basaltic andesite lavas that comprise the Santa María composite volcano, Guatemala provide a backdrop for understanding more fully the origin of voluminous dacitic magma that has erupted historically from the same magmatic system.

The Santa María–Santiaguito volcanic complex has a relatively simple history that includes a ~75 kyr period of basaltic andesite cone-growth, followed by repose for ~25 kyr and explosive eruption of dacitic pumice and minor basaltic andesitic scoria and ash in 1902 (Rose 1987*a*; Escobar-Wolf *et al.* 2010; Singer *et al.* 2011). By some estimates the 24 October 1902 eruption of Santa María was the third most deadly of the twentieth century, with more than 8750 casualties (Witham 2005). Subsequent eruptions that began in 1922, and which continue to the present day, comprise dacitic lava and ash that occasionally contain quenched mafic inclusions (Rose 1987*a, b*; Harris *et al.* 2003; Escobar-Wolf *et al.* 2008). Whereas Singer *et al.* (2011) used whole rock major and trace element geochemical data, as well as Sr, Pb, Nd, and U–Th isotope compositions to investigate the evolution of basaltic andesite lavas that formed the Santa María cone, this paper focuses on the origin of the historically-erupted dacitic tephra and lava and its relationship to cone-forming mafic magmas that preceded the dacite. In addition to new whole rock major and trace element and Sr–Nd–Pb–O isotope compositions from these historically erupted materials, we present the composition of phenocryst minerals including zoning in plagioclase obtained via electron probe micro-analysis (EPMA), and H_2O concentrations of plagioclase-hosted melt inclusions in dacite pumice determined using secondary ion mass spectrometry (SIMS). These datasets are used collectively to quantify processes that led to the catastrophic eruption of 1902.

Geological and petrologic background

Subduction of the Cocos plate at 7–8 cm/yr beneath the Caribbean plate has generated the Central American Volcanic Arc (CAVA) between Guatemala and Costa Rica. Volcán de Santa María, near the western end of the CAVA, is one of 39 centers that define the arc front which is 165–190 km from the Middle America Trench (Fig. 1). Crustal thickness beneath the arc varies from >40 km at its northwestern (Guatemala) and southeastern (Costa Rica) ends, to ~30 km beneath its centre in Nicaragua (Carr 1984; Carr *et al.* 2003, 2007). Volcán de Santa María sits atop the Chortis block that includes mainly poorly exposed Palaeozoic metamorphic rocks, but also Cretaceous ophiolites which crop out along the Motagua fault north of the volcano (Fig. 1; Beccaluva *et al.* 1995). The surface of the Chortis block is widely capped with several hundred metres of undivided volcanic rocks of late Cenozoic age that include deeply eroded remnants of Pleistocene andesite volcanoes which crop out beneath the Santa María cone (Fig. 2).

The majority of geochemical data within the CAVA are from lavas erupted in the central and southern parts of the arc. Beneath Guatemala the crust is thicker and more lithologically diverse which allows for a potentially more complex evolution of magma (e.g. Rose 1987*a*; Halsor & Rose 1988; Vogel *et al.* 2006; Walker *et al.* 2007). It has also been proposed by Heydolph *et al.* (2012) that the lithospheric mantle beneath Guatemala is exceptionally heterogeneous, leading to a distinctively 'crustal' isotopic composition of mafic lavas in this part of the CAVA. The Santa María–Santiaguito complex is strongly bimodal both chemically and temporally, having erupted 8 km^3 of basaltic andesite lava (51–56% SiO_2) between 103 and 25 ka, but with dacite (63–67% SiO_2) dominating the >9 km^3 of historically erupted material (Rose 1987*a*; Escobar-Wolf 2010; Singer *et al.* 2011; Fig. 2). The 1902 eruption was itself bimodal with >98% of the airfall deposit comprising dacite pumice and ash overlain by a minor layer of basaltic andesite ash and scoria (Rose 1972; Williams & Self 1982). Lithic fragments of granitoid and metamorphic rocks also comprise several percent by mass of the airfall deposit (Rose 1972). Despite the thick crust beneath Volcán de Santa María, Jicha *et al.* (2010) used Sr and U–Th isotope data to show that the flux of slab fluid into the mantle below Guatemala is equal to, or greater than, in

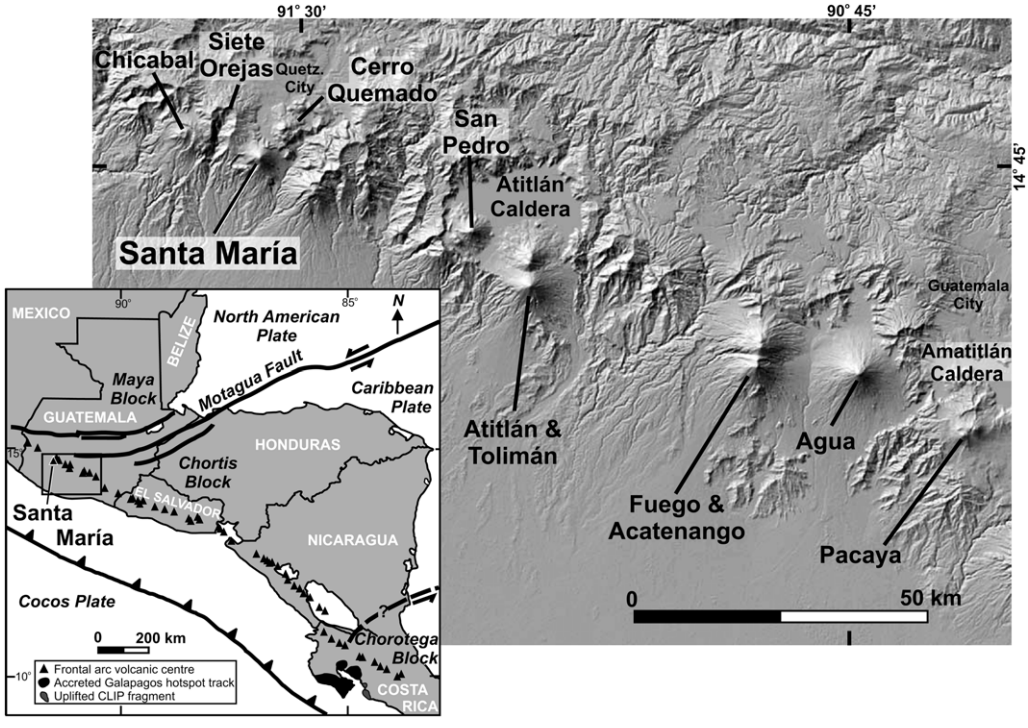

Fig. 1. Digital elevation map of western Guatemala adapted from Escobar-Wolf *et al.* (2010). Quetz., Quetzaltenango. Inset: tectonic setting of Santa María volcano modified from Carr *et al.* (2007*b*) and Geldmacher *et al.* (2008). CLIP, Caribbean Large Igneous Province.

other parts of CAVA where crust is relatively thin (e.g. Nicaragua), a finding that conflicts with other models (Patino *et al.* 2000; Carr *et al.* 2003; Heydolph *et al.* 2012). Moreover, Jicha *et al.* (2010) inferred that a portion of the crust beneath Santa María comprises ancient mid-ocean ridge basalt (MORB) and is not limited to metamorphic and granitic rocks. Singer *et al.* (2011) present major and trace element compositions and Sr, Nd and Pb isotope ratios from 27 basaltic andesite lava flows that comprise a sequence of four cone-building phases, each erupted from a common central summit vent or nearby flank vents, that have been dated using the $^{40}Ar/^{39}Ar$ method at between 103–72, 72, 60–46 and 35–25 ka. Thus the entire period of mafic cone-building spanned about 75 kyr. Energy-constrained, recharge, assimilation-fractional crystallization modelling (EC-RAFC; Spera & Bohrson 2004; Bohrson & Spera 2007) reveals that during the initial phases of cone growth between about 103 and 35 ka, repeated recharge of a deep magma reservoir system with basalt was likely an important process that modulated the trace element and isotopic composition of erupted lavas. Moreover, the same EC-RAFC modelling suggests that the episodic addition of recharge magma to the mass of magma evolving within the deep crustal storage zone augmented latent heat being released by crystallization, thereby amplifying the role of partial melting and assimilation during the final phase of cone growth 35–25 ka (Singer *et al.* 2011).

Samples and analytical methods

During field campaigns totalling 20 days in 2005, 2007 and 2009, samples were collected from the 1902 airfall deposit and the Santiaguito dome complex. Dacite pumice blocks, scoria lapilli, and angular lithic fragments of granitoid were collected in stratigraphic sequence from three road cuts through the 1902 airfall deposit, including site SM-07-09 that lies 4 km NW of the 1902 crater (14°46.560′N, 91°34.480′W, 2631 masl) where the deposit is 95 cm thick, site SM-09-16 that is 8 km SW of the crater (14°42.905′N, 91°37.321′W, 1190 masl) where the deposit is 160 cm thick, and at site SM-05-1902 about 3 km from the crater (14°46.239′N, 91°35.014′W, 2570 masl) where only dacite pumice was collected (Fig. 2). In addition, samples were collected from seven of the

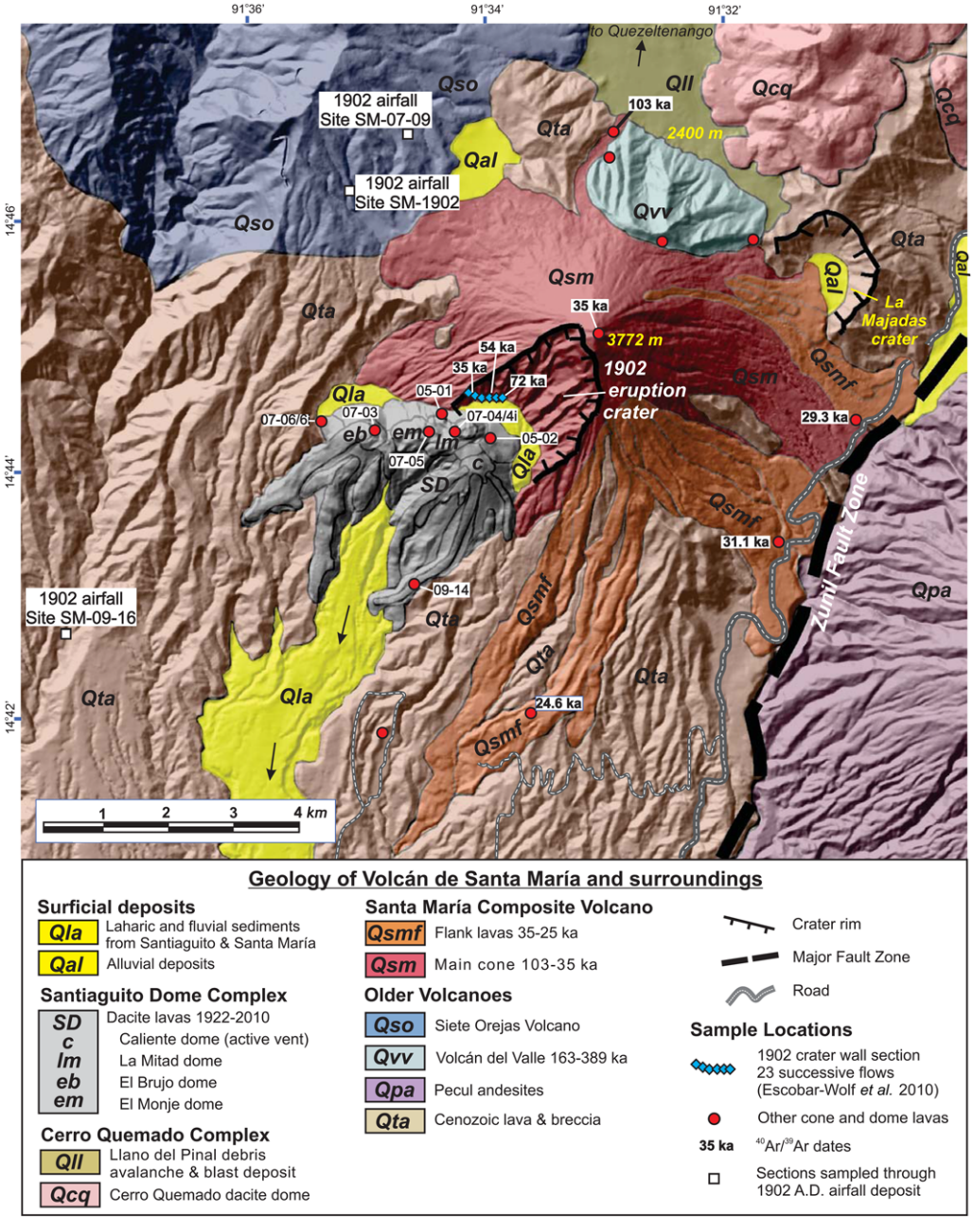

Fig. 2. Geological map of the Santa María-Santiaguito volcanic system, modified from Escobar-Wolf *et al.* (2010).

more than 30 dacite lava flows that comprise the Santiaguito dome complex, including three lavas erupted between 1939 and 1942 on the La Mitad dome, one from a 1950 eruption of the El Monje dome, two lavas from the El Brujo dome (1972 and 1973 flows), and two samples from the Caliente dome, including a 1972 flow and one from a flow resulting from an eruption in 2002 at the currently active vent (Fig. 2). Portions of the 1939 dacite flow on La Mitad contained dark coloured, fine-grained inclusions of basaltic andesite, 1–10 cm across and with crenulated margins

that appear to have quenched glassy rims (Rose 1987*a*), as did the 1972 flow from El Brujo. We collected several inclusions from these two localities for analysis.

Whereas Santa María cone lavas are highly porphyritic, two-pyroxene olivine-bearing basaltic andesites, dacite pumice in 1902 airfall deposit contains up to 20% phenocrysts of clinopyroxene, orthopyroxene, amphibole, plagioclase, iron titanium oxides, and trace zircon. The basaltic andesite scoria is petrographically similar to the cone-forming lavas with the exception that some scoria lapilli contain minor amphibole phenocrysts. Dacites from Santiaguito dome complex are slightly less SiO_2-rich than the 1902 pumice and contain a higher modal percent of the same phenocryst minerals found in the pumice (Rose 1972, 1987*a*).

Review of Santa María geochemistry

The major and trace element compositions and Sr, Nd and Pb isotope ratios from 27 basaltic andesite lava flows that comprise the Santa María composite cone were presented by Singer *et al.* (2011). In order to emphasize the profound compositional and temporal bimodality of the entire Santa María–Santiaguito complex, Singer *et al.* (2011, figs 5 & 6) compared these 27 mafic cone-forming lavas to the historically-erupted dacite tephra and lavas in variation diagrams. The major and trace element compositions from whole rock samples of the historically-erupted materials described in the previous section, including pumice, scoria and lithic fragments collected from the 1902 airfall deposit, and from each of the major phases of the Santiaguito dome complex, plus quenched mafic inclusions in two of the dacite lava domes, are presented in this paper. From a subset of these whole rock samples we also present new Sr, Nd and Pb isotope ratios and $\delta^{18}O$(WR) values. Jicha *et al.* (2010) present whole rock $^{238}U-^{230}Th$ isotope compositions from Santa María cone-forming lavas, the 1902 dacite pumice and basaltic andesite scoria, and several Santiaguito dacite dome lavas. Here we report new $^{238}U-^{230}Th$ isotope compositions from minerals and glass separated from the 1902 dacite pumice and from a dacitic lava that erupted in 1972 to form part of the El Monje dome in the Santiaguito dome complex.

Whole rock major and trace element analyses

Twenty-nine whole rock samples (including three glass separates from 1902 pumice) of 250–500 g each were crushed (tungsten-carbide piston crusher), powdered (aluminum oxide ceramic shatterbox and puck), and analysed for major (X-ray fluorescence) and trace elements (inductively-coupled plasma mass spectrometry, ICP-MS) at the Open University, UK following methods of Rogers *et al.* (2006). Details on procedures including precision and accuracy are provided in Singer *et al.* (2011).

Pb, Sr and Nd isotopes

A representative subset of the whole rock samples were analysed for $^{87}Sr/^{86}Sr$ (18 samples), $^{208}Pb/^{204}Pb$, $^{207}Pb/^{204}Pb$, $^{206}Pb/^{204}Pb$ (14 samples) and $^{143}Nd/^{144}Nd$ (17 samples) at the UW-Madison Radiogenic Isotope Laboratory via thermal ionization mass spectrometry (TIMS, Micromass Sector 54 instrument). Analytical procedures follow those described in Singer *et al.* (2011). For Pb isotope analyses, instrumental mass bias was corrected empirically based on analyses of NIST SRM-981 ($n = 10$) and SRM-982 ($n = 11$) run under similar conditions as samples. The pooled average mass fractionation correction based on the measured $^{207}Pb/^{206}Pb$ analysis of SRM-981 and the measured $^{208}Pb/^{206}Pb$ ratio of SRM-982 was 0.00148 $\pm$ 0.00045 per amu. Strontium and neodymium isotope measurements were exponentially corrected for mass fractionation using $^{86}Sr/^{88}Sr = 0.1194$ and $^{146}Nd/^{144}Nd = 0.7219$, respectively. Repeat analysis of NIST SRM-981 yielded an average $^{87}Sr/^{86}Sr$ ratio of 0.710267 $\pm$ 0.000018 (2-SD; $n = 30$). Duplicate samples of the USGS rock standard BCR-1 were processed through the entire analytical procedure and the measured $^{87}Sr/^{86}Sr$ ratios were 0.705021 and 0.705028. The measured $^{143}Nd/^{144}Nd$ for two in-house Nd standards (Ames I and Ames II) are 0.512149 $\pm$ 0.000014 ($n = 15$; 2-SD) and 0.511974 $\pm$ 0.000016 ($n = 15$; 2-SD), respectively. The measured $^{143}Nd/^{144}Nd$ for La Jolla Nd was 0.511844 $\pm$ 0.000015 ($n = 6$; 2-SD). Duplicate samples of the USGS rock standard BCR-1 measured $^{143}Nd/^{144}Nd$ ratios were 0.512920 $\pm$ 0.000010 and 0.512908 $\pm$ 0.000008 (errors are 2-SE in-run statistics).

U and Th isotopes

In addition to two whole rock samples of dioritic lithic fragments in the 1902 airfall deposit, minerals and glass separated from 1902 dacite pumice sample SM-07-09B and dacite lava sample SG-05-01 from the Mitad dome, were analysed for U–Th isotope composition. Solution-based U and Th isotope measurements were obtained using a Micromass *Isoprobe* multi-collector ICP-MS at UW-Madison's Radiogenic Isotope Laboratory using procedures of Jicha *et al.* (2009). Rock

standards including AThO, BCR-1, and AGV-1 were analysed along with variable concentration IRMM-035 and IRMM-036 solutions to monitor accuracy, reproducibility and external precision (details in Singer *et al.* 2011). The mean $^{232}Th/^{230}Th$ values for IRMM 035 (87 799 $\pm$ 1006; 2-SD; $n = 15$) and IRMM 036 (326 300 $\pm$ 2126; 2-SD; $n = 8$) are indistinguishable from consensus values (Sims *et al.* 2008).

O isotopes

Whole rock powders were analysed at the University of Wisconsin-Madison by laser fluorination (Valley *et al.* 1995) using an air-lock sample chamber (Spicuzza *et al.* 1998) with bromine pentafluoride as the reagent and a 25W CO_2 laser. Isotope ratios were measured using a Finnigan MAT 251 dual inlet mass spectrometer. Whole rock $\delta^{18}O$ values were standardized using standard UWG-2 garnet (accepted $\delta^{18}O = 5.80‰$ VSMOW; Valley *et al.* 1995). Eight standards run on each day of analysis (three days total) yield a reproducibility of $< \pm 0.16‰$ (2 std. dev.). The average difference in $\delta^{18}O$ value between duplicate analyses of whole rock powders was $< 0.08‰$.

Electron probe microanalysis of phenocryst minerals

Epoxy mounts were prepared with separates of plagioclase, iron–titanium oxides, pyroxenes and amphibole phenocrysts from 1902 dacite pumice sample SM-07-09B and scoria sample SM-7-09E. Phenocrysts and their melt inclusions were imaged in back-scattered electron (BSE) mode on the Hitachi S-3400N Variable Pressure Scanning Electron Microscope (VP-SEM) at the University of Wisconsin-Madison. Energy Dispersive Spectrometry (EDS) located grains of specific minerals (e.g. orthopyroxene v. clinopyroxene or ilmenite v. titanomagnetite) which then were analysed by Wavelength Dispersive Spectrometry (WDS) on the Cameca SX51 5-spectrometer electron microprobe at UW-Madison. Major element compositions of minerals were obtained using a 1 μm diameter beam with an accelerating potential of 15 keV. Natural and synthetic standards of olivine, pyroxene, plagioclase, amphibole and iron–titanium oxides were used for calibration. Automation and data reductions used Probe for Windows software with the matrix correction of Armstrong (1988). In anticipation of element migration under a focused electron beam (Morgan & London 1996), analyses of plagioclase-hosted melt inclusions employed time-integrated intensities collected at 2 s intervals for 20 s, allowing Na, K and Si concentrations in the glass to be extrapolated to a time-zero value. To obtain a large number of anorthite content profiles of plagioclase phenocrysts, we used greyscale values from the BSE images as a proxy for An content generally following the procedures outlined by Ginibre *et al.* (2002) and Triebold *et al.* (2006). The An profiles were calibrated via WDS analyses of 10 points along each profile.

Secondary Ion Mass Spectrometry (SIMS) analysis of trace elements in plagioclase

Polished gold-coated epoxy mounts of plagioclase crystals were analysed for K, Mg, Ti, Fe, Sr and Ba using the Cameca ims-1280 ion microprobe at the WiscSIMS Laboratory, UW-Madison. The analysis conditions are after Kita *et al.* (2004) using high mass resolution mode (mass resolving power of 5000) without energy filtering. The primary beam of O^- ions with 1 nA intensity was focused to a spot of *c.* 10 μm in diameter at the sample surface. For each element, secondary ion intensity was normalized to the intensity of the $^{30}Si^+$ ions. A natural plagioclase standard with known trace element concentrations (Lab1, Kita *et al.* 2004) was analysed multiple times in the same analytical session, from which relative sensitivity factors of each element were determined. Reproducibility of ratios between respective ions and $^{30}Si^+$ of repeated analyses of plagioclase standard was better than 3% (1σ).

SIMS analysis of plagioclase-hosted melt inclusions

In polished, gold-coated epoxy mounts 2 mm thick, melt inclusions ranging from 30–100 μm across in plagioclase from 1902 dacite pumice sample SM-07-09B were analysed for hydrogen using the Cameca IMS-1280 ion microprobe at the WiscSIMS Laboratory, UW-Madison. A primary beam of Cs^+ (20 keV impact energy and 0.6 nA beam current) was focused to a spot of ~8 μm at the sample surface and a normal incidence electron gun was used for charge compensation. General instrument parameters are similar to that of oxygen isotope analysis (Kita *et al.* 2004). The negative secondary ions of H^- and $^{30}Si^-$ were measured using the axial electron multiplier in single collection mode. In order to precisely aim at these melt inclusions, we obtained secondary H^- ion images of the sample surface by rastering the primary beam over a 50 × 50 μm areas for three minutes and identified the location of melt inclusions from a hot spot of high H^- count rates. Subsequently, we used a stationary primary beam centred on the melt inclusion and detected secondary H^- and $^{30}Si^-$

ions that were emitted from only the central 2 μm squares of the sputtered area by using a field aperture with opening of 400 × 400 μm (magnification of transfer optics was ×200 from sample to the field aperture). Mass resolving power was set to 3000. The secondary H^- ion intensities were normalized to that of the $^{30}Si^-$ ion and the $H^-/^{30}Si^-$ ratios were obtained after correction for hydrogen background as measured several times on the host plagioclase crystals between measurement of the melt inclusions.

The seven rhyolite glasses used as standards for the hydrogen measurements were produced experimentally from a sample of a natural obsidian flow, and contain between 0.1 and 6.1 wt% H_2O (Tenner *et al.* 2010). Electron probe major element compositions, and SIMS data from these glasses can be found in the Supplementary material. The glass standards were analysed multiple times during the analytical session to generate a calibration curve for $H^-/^{30}Si^-$ ratios (Supplementary material). Following SIMS analysis, the SiO_2 content of each analysed inclusion was measured by electron probe and the calibration curve was used to estimate the wt% H_2O with a precision of about ±3% (1σ; Supplementary material).

Results

Major and trace elements and Sr–Nd–Pb–O isotopes

The whole rock major and trace element concentrations and Sr, Nd, and Pb isotope ratios are summarized in Table 1. The O isotope results from the whole rock samples of this study, as well as samples of the cone-forming basaltic andesite lavas measured for elemental concentrations and Sr–Nd–Pb isotope ratios by Singer *et al.* (2011), are summarized in Table 2. Representative plots of K_2O, MgO, Th, Sr, $^{87}Sr/^{86}Sr$, $^{143}Nd/^{144}Nd$, $^{206}Pb/^{204}Pb$ and $\delta^{18}O$(WR) v. SiO_2 serve to illustrate the major geochemical and isotopic features of the 1902 eruptive products and to contrast these with the preceding Santa María cone-forming lavas and the subsequently erupted Santiaguito dome lavas (Fig. 3). In the 1902 airfall deposit, dacite pumice contains 64.6 to 67.2 wt% SiO_2, whereas the basaltic andesite scoria has 53.9 to 55.9 wt% SiO_2, thus revealing the strongly bimodal nature of the 1902 magma body distinguished by a >10% gap in SiO_2. Rhyodacitic glass separated from three dacite pumice blocks contains 67.8 to 70.4 wt% SiO_2 and is richer in K_2O and Th (and other incompatible elements) and poorer in MgO and Sr on average (and other compatible elements) than the bulk dacite pumice (Fig. 3). The 1902 scoria is similar in major and trace element composition to the more SiO_2-rich of the basaltic andesite lava flows that erupted during the latest cone-forming phase of Santa María volcano between 35 and 25 ka. Lavas comprising the Santiaguito dome complex contain less SiO_2, 62.4 to 64.7 wt%, compared to the 1902 dacite pumice and the quenched inclusions we have measured from two of these flows are remarkably similar to the 1902 scoria with respect to major and trace element composition (Fig. 3). The six fine- to medium-grained diorite to granodiorite lithic fragments we chose to analyse from the 1902 deposit range from 48 to 60% SiO_2 and, with the exception of MgO, are not collinear with the basaltic andesitic cone-lavas of Santa María volcano, instead being scattered with no simple relationship to the volcanic rocks. These results are consistent with, and reinforce, the observations of Rose (1987*a*) regarding the bimodality of the volcano, and the similarity among mafic and silicic magmas over time. However, owing to vast improvements in analytical precision during the last three decades, and a larger number of measurements than obtained by Rose *et al.* (1977), the Sr, Nd and Pb isotope results we have obtained reveal several previously unappreciated features of this system.

The $^{87}Sr/^{86}Sr$ ratios of 0.703848 and 0.703880 obtained from two blocks of 1902 dacite pumice are similar to that of 0.703837 in the glass separated from a third block; however, these ratios are significantly lower than ratios that range from 0.703897 to 0.703950 obtained from four scoria lapilli from the same eruption (Fig. 3). The Santiaguito dacite lavas (and quenched mafic inclusions) erupted in 1939 from the Mitad dome, 1972 from El Brujo, 1972 and 2002 from Caliente, have $^{87}Sr/^{86}Sr$ ratios similar to those of the 1902 dacite pumice; however, lavas from the eruptions in 1950 of El Monje, and 1973 of El Brujo are significantly higher at 0.703905 and 0.703977, respectively (Fig. 3). Notably, the entire range of $^{87}Sr/^{86}Sr$ ratios found in the rhyodacite glass, dacite pumice and dacite lava flows erupted in 1902 and afterward is comparable to that of the basaltic andesite lavas that erupted 35–25 ka during the late phase of Santa María cone growth (Fig. 3). With one exception, the diorite–granodiorite lithic fragments span this same range. For the most part $^{143}Nd/^{144}Nd$ ratios mirror those of $^{87}Sr/^{86}Sr$. The 1902 rhyodacite glass has a higher $^{143}Nd/^{144}Nd$ ratio than the dacite pumice, whereas pumice has a similar ratio to three of the four scoria samples. The 1902 scoria and quenched basaltic andesite inclusion from the 1939 La Mitad dome lava span a range of $^{143}Nd/^{144}Nd$ ratios comparable to those of the basaltic andesitic lavas that erupted 35–25 ka during the late phase of Santa María cone growth.

Table 1. *Major and trace element, and Sr, Nd and Pb isotope data from whole rock and glass samples in 1902 airfall deposit and Santiaguito dome lavas*

	1902 Plinian eruption								
Sample unit name type	SM-07-09A 1902 airfall pumice block	SM-07-09B 1902 airfall pumice block	SM-1902 1902 airfall pumice block	SM-09-16A 1902 airfall pumice block	SM-09-16B 1902 airfall pumice block	SM-07-09G 1902 airfall pumice block	SM-07-09Bg 1902 airfall pumice glass	SM-09-16Ag 1902 airfall pumice glass	SM-09-16Bg 1902 airfall pumice glass
SiO_2 (wt%)	66.19	64.69	66.32	67.23	66.89	64.58	70.43	68.96	67.82
TiO_2	0.32	0.38	0.33	0.30	0.30	0.38	0.27	0.24	0.20
Al_2O_3	16.30	17.11	16.70	16.56	16.46	16.95	14.68	16.16	18.06
Fe_2O_3	3.63	4.40	3.83	3.34	3.34	4.06	2.27	2.10	1.64
MnO	0.14	0.16	0.15	0.14	0.14	0.17	0.12	0.10	0.09
MgO	1.17	1.61	1.24	1.09	1.04	1.49	0.63	0.62	0.49
CaO	3.58	4.48	3.86	3.52	3.49	4.24	2.27	3.04	3.98
Na_2O	4.90	4.93	5.02	4.94	5.00	4.87	4.88	5.08	5.33
K_2O	1.86	1.67	1.80	1.84	1.86	1.70	2.30	2.07	1.80
P_2O_5	0.18	0.19	0.19	0.18	0.18	0.18	0.14	0.15	0.13
LOI	1.29	0.70	0.98	0.97	0.78	0.82	1.34	1.06	0.73
Total	99.56	100.33	100.41	100.09	99.48	99.46	99.33	99.59	100.27
Li (ppm)	24.9	22.8	24.0	24.6	25.1	22.6	29.9	27.4	24.7
Sc	4.26	6.68	4.34	3.53	3.44	6.43	3.39	3.19	2.46
Ti	1973	2363	2025	1766	1775	2317	1627	1473	1150
V	31.9	51.3	35.2	25.8	25.8	53.5	15.1	12.7	9.7
Cr	0.8	2.0	0.6	0.5	0.7	2.7	0.4	6.4	5.4
Mn	1171	1224	1158	1153	1183	1440	937	901	738
Co	5.5	7.3	5.3	4.6	4.4	24.9	2.9	2.8	2.2
Ni	0.6	1.6	0.4	0.2	0.4	2.2	0.7	0.7	0.4
Cu	8.8	16.8	8.1	10.2	11.2	51.1	14.0	14.8	8.6
Zn	90	99	90	89	91	91	79	73	57
Ga	17.7	18.8	17.8	18.0	18.2	18.1	16.4	17.2	18.4
Rb	37.1	32.1	34.9	36.7	37.3	33.1	46.6	41.8	35.5
Sr	409	460	434	421	427	451	257	358	495
Y	17.1	17.0	16.8	16.5	16.5	16.7	18.8	17.5	14.4
Zr	148	135	144	147	147	136	188	167	141
Nb	4.76	4.50	4.56	4.70	4.85	4.37	5.92	5.27	4.48
Mo	0.60	1.53	0.57	0.59	0.61	0.65	0.77	0.68	0.57
Sn	1.09	1.08	0.85	0.97	1.01	0.98	1.45	1.14	0.96
Sb	0.479	0.489	0.452	0.488	0.483	0.211	0.589	0.535	0.484
Cs	1.87	1.69	1.74	1.83	1.83	1.64	2.33	2.10	1.78
Ba	855	828	827	861	873	800	1028	953	860
La	15.22	14.09	14.71	15.12	15.13	14.19	17.27	16.12	14.37
Ce	31.22	29.23	30.26	30.80	30.92	30.12	35.51	33.06	28.79
Pr	4.11	3.93	4.00	4.02	4.06	3.86	4.59	4.28	3.67
Nd	15.87	15.34	15.56	15.60	15.55	15.19	17.46	16.32	13.94
Sm	3.19	3.15	3.09	3.07	3.07	3.11	3.41	3.24	2.69
Eu	0.89	0.91	0.89	0.87	0.87	0.92	0.81	0.85	0.85
Gd	2.82	2.79	2.79	2.73	2.74	2.79	3.00	2.82	2.36
Tb	0.43	0.44	0.44	0.43	0.42	0.44	0.47	0.44	0.37
Dy	2.57	2.60	2.55	2.50	2.48	2.57	2.78	2.58	2.16
Ho	0.55	0.56	0.54	0.54	0.53	0.55	0.60	0.56	0.46
Er	1.66	1.64	1.62	1.60	1.60	1.63	1.83	1.69	1.40
Yb	1.81	1.76	1.75	1.78	1.76	1.74	2.07	1.90	1.57
Lu	0.30	0.28	0.28	0.29	0.29	0.29	0.34	0.32	0.26
Hf	3.59	3.45	3.49	3.55	3.58	3.29	4.56	4.00	3.38
Ta	0.29	0.28	0.28	0.29	0.29	0.26	0.35	0.31	0.39
Pb	9.12	9.60	8.73	9.15	9.22	8.33	12.74	10.16	9.06
Th	2.43	2.24	2.33	2.42	2.43	2.18	3.08	2.74	2.31
U	1.00	0.94	0.96	1.00	1.01	0.89	1.26	1.17	0.97
$^{206}Pb/^{204}Pb$		18.717			18.702				18.700
$^{207}Pb/^{204}Pb$		15.592			15.593				15.590
$^{208}Pb/^{204}Pb$		38.432			38.450				38.438
$^{87}Sr/^{86}Sr$		0.7038799			0.7038477				0.7038372
$\pm 2\sigma$		0.000011			0.000020				0.000020
$^{143}Nd/^{144}Nd$		0.5129115			0.5129195				0.5129372
$\pm 2\sigma$		0.000009			0.000010				0.000008

The lithic fragments have higher $^{143}Nd/^{144}Nd$ ratios than any of the volcanic rocks (Fig. 3). The $^{206}Pb/^{204}Pb$ ratios of 18.70–18.72 for the 1902 dacite pumice and rhyodacite glass separated from it are slightly higher on average than those of the two scoria samples, 18.68–18.70, and as seen for the other isotopes, all the historically-erupted materials fall within the range spanned by the latest cone-forming basaltic andesite lavas erupted 35–25 ka on Volcán de Santa María (Fig. 3). The lithic fragments have $^{206}Pb/^{204}Pb$ ratios that fall at the higher end of the range defined by the volcanic rocks.

The $\delta^{18}O$(WR) values of 6.25 to 6.42‰ for most of the cone-forming basaltic andesite lavas correlate positively with SiO_2, whereas the youngest of these lavas from the summit of the cone that is $^{40}Ar/^{39}Ar$-dated at ~35 ka (Escobar-Wolf *et al.*

1902 Plinian eruption										
SM-07-09E 1902 airfall scoria	SM-09-07 1902 airfall scoria	SM-09-16D 1902 airfall scoria	SM-09-16F 1902 airfall scoria	SM-09-16H 1902 airfall scoria	SM-07-09F 1902 airfall lithic frag	SM-07-09H 1902 airfall lithic frag	SM-09-16C1 1902 airfall lithic frag	SM-09-16C2 1902 airfall lithic frag	SM-09-16C3 1902 airfall lithic frag	SM-09-16C4 1902 airfall lithic frag
53.52	54.44	54.40	55.90	53.93	54.52	55.73	53.38	52.96	48.04	60.02
0.92	0.87	0.90	0.81	0.89	1.18	1.26	0.97	0.87	0.79	0.71
19.25	18.66	18.63	18.26	18.44	17.59	16.73	18.63	19.61	16.37	17.60
8.54	8.35	8.46	7.67	8.55	8.86	9.46	8.67	8.56	10.94	6.03
0.14	0.15	0.14	0.13	0.14	0.15	0.19	0.16	0.16	0.18	0.11
4.27	4.04	3.99	3.73	4.47	3.94	3.63	4.10	4.39	9.05	2.40
8.32	7.83	7.84	7.07	7.94	6.81	6.67	7.01	7.55	8.21	5.17
3.55	3.60	3.55	3.74	3.63	4.66	4.13	4.42	4.66	2.50	4.90
1.01	1.11	1.15	1.31	1.10	1.84	1.71	1.40	1.36	2.02	2.08
0.18	0.20	0.20	0.20	0.20	0.40	0.51	0.29	0.27	0.17	0.22
0.41	0.70	0.68	0.62	0.67	0.31	0.17	0.34	0.17	1.29	0.35
100.10	99.94	99.95	99.44	99.97	100.27	100.18	99.36	100.55	99.55	99.58
10.6	11.8	12.2	14.8	11.5	14.0	13.5	19.2	8.4	25.7	16.7
26.69	23.74	23.75	21.00	23.71	23.63	29.67	24.89	26.36	26.70	16.12
5988	5113	5444	5003	5270	7139	8367	7041	5159	4579	4221
250.8	197.6	210.9	176.6	206.4	227.7	243.2	224.9	199.2	219.7	114.8
36.1	31.6	42.7	31.1	48.2	46.7	48.8	39.9	46.6	129.9	6.4
1107	1178	1107	1091	1168	1165	1589	1359	1295	1458	912
28.9	28.5	28.8	24.5	30.3	25.4	26.9	28.7	26.1	59.5	16.2
22.6	15.5	21.0	14.8	20.4	27.5	27.8	17.9	19.6	163.0	6.2
78.7	88.2	74.9	59.8	67.2	93.8	232.3	156.0	38.4	101.8	34.3
96	95	92	92	97	117	147	100	95	98	74
20.8	19.5	19.6	19.7	19.5	20.9	20.3	20.8	22.4	17.2	20.3
19.1	20.9	22.0	27.5	19.9	37.8	48.6	27.4	29.3	50.0	41.0
545	521	513	516	528	424	381	486	525	356	413
19.4	19.8	18.9	18.6	18.6	26.4	38.1	23.6	25.0	21.3	19.9
105	104	108	116	110	5	9	5	8	21	4
3.25	3.12	3.13	3.80	3.12	7.13	8.98	6.51	4.38	4.11	4.74
0.98	0.38	0.38	0.41	0.37	1.10	1.90	0.24	0.37	0.10	1.26
1.12	1.05	0.70	1.15	1.04	1.38	1.83	0.82	1.66	0.97	1.09
0.245	0.236	0.212	0.252	0.207	0.325	0.133	0.427	0.034	0.114	0.389
0.88	1.01	0.96	1.26	0.87	1.31	1.15	1.49	0.78	2.18	1.98
524	511	520	586	510	728	688	666	512	465	837
9.24	9.73	9.78	11.15	9.58	13.71	19.99	13.76	13.93	8.01	12.95
20.65	21.03	21.15	23.82	20.70	28.65	45.36	29.28	30.79	20.43	26.46
2.98	3.05	3.08	3.38	3.00	4.85	6.51	4.11	4.36	3.08	3.63
13.03	13.37	13.45	14.30	13.28	21.49	27.93	17.64	18.61	13.09	15.35
3.26	3.29	3.32	3.35	3.25	5.15	6.51	4.12	4.30	3.18	3.61
1.01	1.01	1.02	1.01	1.00	1.23	1.48	1.16	1.21	0.90	1.08
3.28	3.35	3.38	3.34	3.31	5.00	6.48	4.18	4.22	3.25	3.54
0.53	0.54	0.55	0.53	0.52	0.78	1.03	0.66	0.68	0.54	0.56
3.18	3.23	3.17	3.09	3.10	4.68	6.13	3.89	4.00	3.28	3.34
0.67	0.67	0.66	0.65	0.64	0.99	1.29	0.82	0.86	0.72	0.70
1.89	1.93	1.87	1.83	1.82	2.77	3.64	2.33	2.47	2.12	1.99
1.75	1.83	1.74	1.75	1.68	2.49	3.31	2.15	2.33	2.28	1.84
0.26	0.28	0.27	0.27	0.27	0.36	0.49	0.33	0.36	0.36	0.28
2.71	2.58	2.72	2.89	2.67	0.31	0.32	0.28	0.50	1.04	0.21
0.19	0.18	0.18	0.22	0.18	0.40	0.59	0.37	0.33	0.27	0.25
6.12	5.36	5.43	6.30	5.31	7.91	8.41	5.59	5.47	2.63	6.64
1.19	1.34	1.57	1.89	1.24	1.72	2.39	0.79	1.37	1.00	0.55
0.47	0.54	0.62	0.75	0.51	0.42	0.86	0.31	0.40	0.48	0.24
18.708		18.685			18.751	18.720	18.713			
15.605		15.588			15.594	15.587	15.587			
38.494		38.425			38.502	38.463	38.462			
0.7039014		0.7039406	0.7039497	0.7038965	0.7039923	0.7038872	0.7037453			0.7038652
0.000010		0.000020	0.000020	0.000020	0.000014	0.000010	0.000023			0.000023
0.5129212		0.5128925	0.5129082	0.5129150	0.5129415	0.5129410	0.5129679			0.5129680
0.000008		0.000008	0.000008	0.000008	0.000010	0.000009	0.000008			0.00009

2010; Singer *et al.* 2011) has a much higher value of 6.95‰ (Fig. 3). In the 1902 deposit the basaltic andesite scoria has a $\delta^{18}O$ of 6.54‰ and the dacite pumice is 6.95‰; the latter is identical to that of the youngest cone lava. The Santiaguito dacite dome lavas have $\delta^{18}O$ between 6.55 and 6.82‰, whereas the quenched basaltic andesite inclusions in two of these lavas are 6.50 and 6.60‰ (Fig. 3), similar to the 1902 scoria. The $\delta^{18}O$ values are inversely correlated with $^{87}Sr/^{86}Sr$ such that the early cone lavas have lower $\delta^{18}O$ and higher $^{87}Sr/^{86}Sr$ than the youngest cone lavas and the dacites that erupted long after cone growth ceased (Fig. 4).

U–Th isotopes

Whole rock ($^{238}U/^{232}Th$) and ($^{230}Th/^{232}Th$) activity ratios of nine historically erupted dacite

Table 1. *Major and trace element, and Sr, Nd and Pb isotope data from whole rock and glass samples in 1902 airfall deposit and Santiaguito dome lavas (Continued)*

	Santiaguito Dome lavas							Mafic inclusions	
Sample unit name type	SM-07-04 Mitad 1939 lava	SG-05-01 Brujo 1947 lava	SM-07-05 Monje 1950 lava	SM-07-06 Brujo 1972 lava	SG-05-02 Cal 1972 lava	SM-07-03 Brujo 1975 lava	SM-09-14 2002 flow lava	SM-07-04i Mitad 1939 inclusion	SM-07-06i Brujo 1972 inclusion
SiO_2 (wt%)	63.01	64.44	64.16	63.75	64.65	63.39	62.38	55.28	54.90
TiO_2	0.52	0.39	0.44	0.49	0.51	0.46	0.55	0.89	0.88
Al_2O_3	17.59	17.23	17.32	17.41	16.80	17.40	17.79	18.90	18.69
Fe_2O_3	5.24	4.31	4.69	4.98	4.92	4.79	5.33	8.25	8.19
MnO	0.14	0.14	0.14	0.15	0.14	0.14	0.14	0.15	0.15
MgO	1.88	1.50	1.67	1.83	1.68	1.71	2.12	3.23	3.23
CaO	5.23	4.46	4.74	4.93	4.47	4.83	5.48	7.83	7.72
Na_2O	4.85	4.86	4.82	4.82	4.97	4.77	4.71	4.08	3.91
K_2O	1.60	1.71	1.68	1.67	1.82	1.67	1.58	1.20	1.09
P_2O_5	0.24	0.21	0.22	0.22	0.24	0.22	0.23	0.32	0.23
LOI	0.07	0.23	0.13	0.07	0.06	0.10	0.01	0.12	0.94
Total	100.35	99.49	100.03	100.32	100.27	99.47	100.31	100.25	99.93
Li (ppm)	20.7	22.4	21.3	21.2	22.0	21.3	20.4	31.7	24.9
Sc	10.36	6.32	7.98	8.97	8.68	8.37	11.12	21.58	22.83
Ti	3215	2392	2731	2942	3191	2824	3178	5579	5404
V	84.6	48.0	61.3	70.6	76.6	65.6	89.2	200.1	204.5
Cr	1.3	1.6	1.1	1.3	2.3	1.6	4.3	0.6	1.3
Mn	1151	1142	1146	1167	1153	1137	1183	1156	1181
Co	9.4	7.2	8.1	9.2	8.8	8.6	11.8	18.2	19.1
Ni	1.2	3.7	1.0	1.2	1.9	1.1	2.2	1.8	3.7
Cu	10.6	11.0	8.9	13.1	14.5	9.2	34.8	21.1	41.6
Zn	95	90	91	92	93	91	92	101	100
Ga	19.3	18.3	18.6	18.9	19.6	18.6	19.7	20.6	20.2
Rb	21.0	33.7	33.2	32.5	35.5	32.6	31.1	14.8	19.4
Sr	481	465	466	476	436	476	491	509	545
Y	16.8	17.7	18.2	18.5	19.8	18.1	18.5	17.5	19.0
Zr	143	149	150	151	167	149	143	113	109
Nb	6.78	4.52	4.49	4.42	5.16	4.39	4.25	3.53	3.36
Mo	1.44	1.71	0.55	0.53	6.70	0.53	0.50	5.37	5.77
Sn	1.04	1.08	0.91	1.03	1.21	1.02	1.07	1.31	1.11
Sb	0.430	0.441	0.418	0.263	0.505	0.434	0.386	0.325	0.290
Cs	1.47	1.66	1.61	1.56	1.81	1.58	1.46	1.02	1.03
Ba	784	802	778	766	905	775	736	558	543
La	10.84	14.66	14.36	14.17	15.21	14.25	13.66	8.51	9.87
Ce	23.68	30.32	29.90	29.68	33.00	29.81	28.46	15.74	21.79
Pr	3.44	4.02	4.01	3.95	4.38	3.99	3.84	2.95	3.09
Nd	14.20	15.97	15.92	15.83	17.60	15.91	15.58	13.01	13.39
Sm	3.10	3.30	3.31	3.36	3.72	3.34	3.35	3.23	3.22
Eu	0.90	0.96	0.96	0.97	1.01	0.97	0.99	0.95	0.97
Gd	2.89	3.00	3.04	3.11	3.38	3.05	3.18	3.21	3.23
Tb	0.45	0.47	0.49	0.49	0.53	0.49	0.49	0.52	0.52
Dy	2.76	2.73	2.82	2.89	3.16	2.83	2.91	3.11	3.13
Ho	0.59	0.58	0.60	0.61	0.68	0.60	0.62	0.65	0.67
Er	1.71	1.72	1.77	1.80	1.98	1.77	1.82	1.85	1.88
Yb	1.78	1.82	1.84	1.83	2.03	1.82	1.88	1.75	1.77
Lu	0.28	0.30	0.30	0.29	0.32	0.30	0.29	0.26	0.27
Hf	3.58	3.59	3.59	3.58	4.17	3.56	3.40	2.91	2.80
Ta	0.28	0.27	0.27	0.26	0.32	0.26	0.33	0.20	0.20
Pb	8.94	8.39	8.11	8.11	10.13	8.59	7.86	7.43	6.59
Th	2.07	2.24	2.24	2.19	2.50	2.20	2.04	1.01	1.35
U	0.80	0.92	0.91	0.89	1.06	0.89	0.82	0.48	0.55
$^{206}Pb/^{204}Pb$	18.685		18.692	18.704	18.684	18.724		18.690	
$^{207}Pb/^{204}Pb$	15.572		15.580	15.595	15.589	15.615		15.574	
$^{208}Pb/^{204}Pb$	38.386		38.407	38.464	38.433	38.526		38.391	
$^{87}Sr/^{86}Sr$	0.7038585		0.7039050	0.7038864	0.7038754	0.7039773	0.7038624	0.7038992	
$\pm 2\sigma$	0.000017		0.000008	0.000010	0.000008	0.000010	0.000020	0.000010	
$^{143}Nd/^{144}Nd$	0.5129132			0.5128839	0.5129188	0.5129197	0.5129113	0.5129041	
$\pm 2\sigma$	0.000009			0.000010	0.000011	0.000009	0.000008	0.000009	

pumice, scoria, dacite dome lavas and their inclusions obtained by Jicha *et al.* (2010) are summarized in Table 3 to provide context for mineral data discussed below. These activity ratios, plus those obtained from 13 basaltic andesite lavas erupted on Santa María volcano between 72 and 25 ka (each corrected for time since eruption using the $^{40}Ar/^{39}Ar$ ages; Singer *et al.* 2011), are all in U-excess by between 3 and 26% (Fig. 5). The older cone lavas are on average further from the equiline, lower in the ($^{230}Th/^{232}Th$) activity ratio, and thus exhibit a greater degree of U-excess than most of the younger cone lavas and the historically-erupted materials. The 1902 dacite pumice and five Santiaguito dacite dome lavas have remarkably similar ($^{238}U/^{232}Th$) and ($^{230}Th/^{232}Th$) activity ratios of about 1.26 and 1.16, respectively, whereas the 1902 scoria and basaltic andesite inclusions from two of the dome lavas have slightly lower ($^{230}Th/^{232}Th$) activity ratios

Table 2. *$\delta^{18}O_{SMOW}$ values of whole rock samples from Volcán de Santa María lava flows and tephra and Santiaguito dome lavas*

Sample	Material	wt% SiO_2	$\delta^{18}O_{SMOW}$
SM-05-01	Early cone-lava	52.1	6.25
SM-05-02	Early cone-lava	51.6	6.29
SM-05-04	Early cone-lava	51.4	6.31
SM-05-05	Early cone-lava	52.9	6.35
SM-05-06	Early cone-lava	52.9	6.37
SM-05-07	Early cone-lava	52.7	6.40
SM-05-09	Early cone-lava	53.4	6.42
SM-05-13	Late cone-lava	52.6	6.38
SM-05-15	Late cone-lava	54.1	6.38
SM-05-20	Late cone-lava	54.1	6.44
SM-05-22	Late cone-lava	54.1	6.43
SM-07-01	Late cone-lava	54.7	6.95
SM-07-09E	1902 scoria	53.5	6.54
SM-09-09B	1902 pumice	64.7	6.95
SM-07-04	1939 dome lava	63.0	6.82
SM-07-04i	1939 dome inclusion	55.3	6.50
SM-07-06	1972 dome lava	63.8	6.60
SM-06-06i	1972 dome inclusion	54.9	6.60
SG-05-02	1972 dome lava	64.7	6.68
SM-07-03	1975 dome lava	63.4	6.55

Complete chemical analyses of early and late cone-lavas are in Singer *et al.* (2011). Complete data for historically erupted materials are in Table 1.

of 1.14. Notably the two magmas that plot nearest to the equiline with the lowest U-excesses include those represented by the 1902 scoria, and one of the youngest basaltic andesite lavas of the Santa María cone (sample SM-07-01 of Singer *et al.* 2011) that erupted from a vent near the summit of the volcano at ~35 ka (Fig. 5).

The ($^{238}U/^{232}Th$) and ($^{230}Th/^{232}Th$) activity ratios of glass, magnetite, orthopyroxene, and amphibole from the 1902 dacite pumice and from the 1972 Caliente dacite dome lava are reported in Table 3. The activity ratios of glass, magnetite and orthopyroxene in the 1902 dacite pumice yield an isochron of 1.9 ± 1.2 ka (Fig. 6a), whereas glass, whole rock, magnetite and amphibole from the 1972 Caliente dome lava define an isochron of 9.5 ± 2.5 ka (Fig. 6b). Note that the whole rock samples of the 1902 dacite pumice and mafic scoria plot below the 1.9 ka isochron in such a way as to be consistent with mixing of the mafic and silicic melts as discussed below. We interpret these internal isochrons as estimates of the time since crystallization began in the two dacite magmas (e.g. Condomines *et al.* 2003; Jicha *et al.* 2005).

When acquiring data from basaltic andesite lavas of the Santa María cone, we discovered that $^{87}Sr/^{86}Sr$ ratios are inversely correlated with the activity ratio ($^{238}U/^{230}Th$) which is a measure of U-excess in the magmas prior to eruption (Jicha *et al.* 2010; Singer *et al.* 2011). Moreover, we observe that over the last ~75 kyr $^{87}Sr/^{86}Sr$ ratios have declined, and $\delta^{18}O$ values increased as the magmas evolved in composition such that they appear to be closer to a state of secular equilibrium in the U–Th isotope system. With the exception of the dacite lava from the 1973 El Brujo flow, the historically-erupted 1902 dacite pumice (and glass) and other Santiaguito dacite lavas erupted between 1939 and 1972 plot in the group with the smallest U-excesses, lowest $^{87}Sr/^{86}Sr$ ratios, and highest $\delta^{18}O$ values (Fig. 6). Basaltic andesite magmas that also fall in this group are represented by the 1902 scoria and one of the youngest cone-forming lavas on Santa María that erupted between 35 and 25 ka.

Oxide and pyroxene composition, oxygen fugacity and thermometry

Titanomagnetite and rare ilmenite in the 1902 dacite pumice and basaltic andesite scoria typically occur as small (<30 μm) inclusions within phenocrysts of amphibole and plagioclase. Like Fe–Ti-oxides from some other well-studied volcanoes (Santorini, Mt St Helens, Mt Pelée), ilmenite and titanomagnetite in the 1902 ejecta are relatively homogenous and show none of the zoning observed at the Soufrière Hills Volcano of Montserrat or Mt Unzen of Japan (Nakada & Motomura 1999; Venezky & Rutherford 1999; Pichavant *et al.* 2002; Devine *et al.* 2003). Titanomagnetite–ilmenite pairs in plagioclase or amphibole host crystals that have log(Mg/Mn) satisfying the equilibrium criteria of Bacon & Hirschmann (1988) were used for estimating temperature and fO_2 (Table 4). Hematite contents in ilmenite above 30 wt% led us to use the algorithm of Ghiorso & Sack (1991) to estimate equilibrium temperature and fO_2. Nine oxide pairs from the dacite pumice yield tightly clustered temperatures between 860 and 885 °C and log fO_2 values between −10.2 and −10.6, whereas four pairs in the basaltic andesite scoria reveal a wider range of temperatures between 925 and 1040 °C with log fO_2 values of −8.0 and −9.5. Together, these T–fO_2 estimates form an array comparable to the Ni–Ni–O+2 buffer curve and are thus similar to dacite from Shiveluch and Pinatubo volcanoes, but significantly more oxidized than dacite from Mt St Helens (Hattori 1993; Evans & Scaillet 1997; Blundy *et al.* 2006) and the Valley of 10 000 Smokes (Hildreth 1983) (Fig. 7).

Pyroxene phenocrysts in 1902 dacite pumice include augite (En_{34-44} Fs_{13-20} Wo_{37-48}) and hypersthene (En_{34-44} Fs_{27-37} $Wo_{0.2-2.3}$), whereas

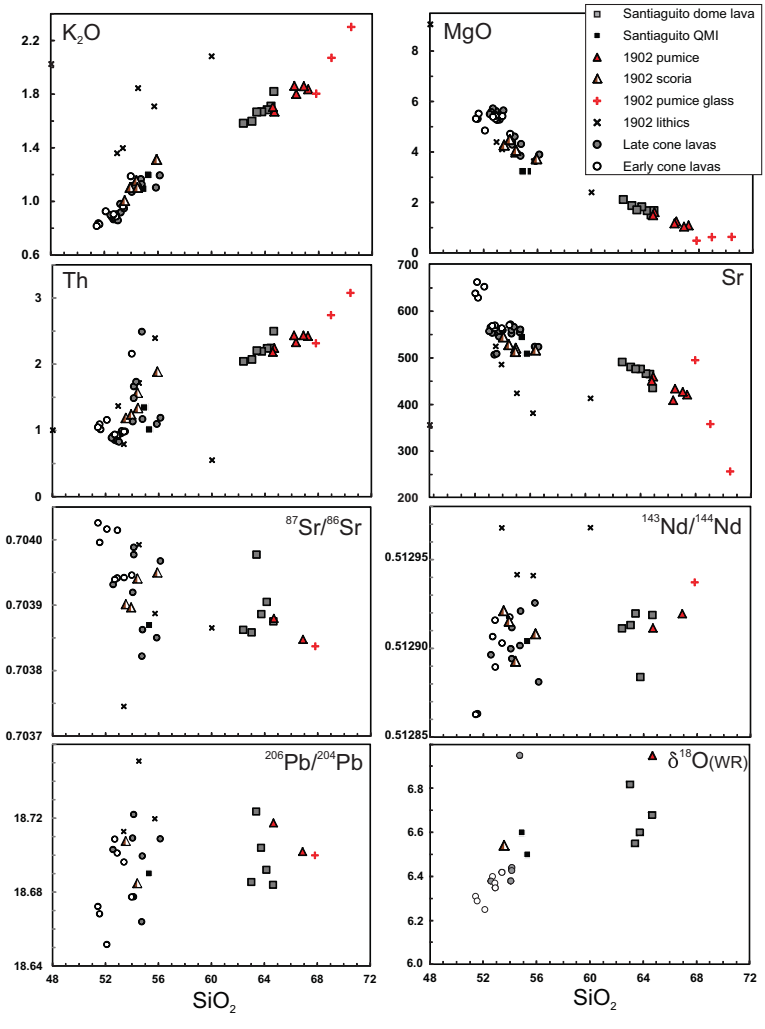

Fig. 3. Variation of selected major elements K_2O and MgO (in wt%), trace elements (in ppm) and Sr, Nd and Pb isotope ratios, and $\delta^{18}O$(WR) values with wt% SiO_2. Diorite and granodiorite fragments from the 1902 airfall deposit are denoted as lithic fragments; quenched mafic inclusions found in Santiaguito dome dacite lavas are denoted as QMI. The major and trace element and radiogenic isotope ratios for the early and late mafic cone lavas (51–55% SiO_2) are from Singer *et al.* (2011).

the basaltic andesite scoria contains augite (En_{38-46} Fs_{10-19} Wo_{39-46}) and bronzite–hypersthene (En_{59-80} Fs_{20-39} $Wo_{0.25-4.0}$); zoning is subtle, <2 mol%, in both minerals (representative analyses in Table 5). As a check on the T–fO_2 estimates from the oxides, temperatures of clinopyroxene and orthopyroxene pairs were estimated using two calibrations of experimental data–one that includes clinopyroxenes with Mg# >0.75 and one that excludes them (Putirka 2008, equations 36 and 37, respectively). Compositions from pyroxene pairs that did not have K_D (Fe–Mg) values within three standard deviations of the equilibrium value of 1.09 ± 0.014 were not used to calculate temperatures, and if the two calibrations were within the ± 30 °C uncertainty of one another, the average temperature was taken as representative (Table 5). The two-pyroxene temperatures are consistent with those estimated from the two-oxide pairs, suggesting that pyroxene crystallized between 750 and 870 °C in the dacite and between 890 and 1000 °C in the basaltic andesite (Fig. 7). The range of two-pyroxene temperatures to values lower than those recorded by the oxides likely reflects Fe–Mg diffusion and partial re-equilibration during magma ascent that did not affect the iron–titanium oxide

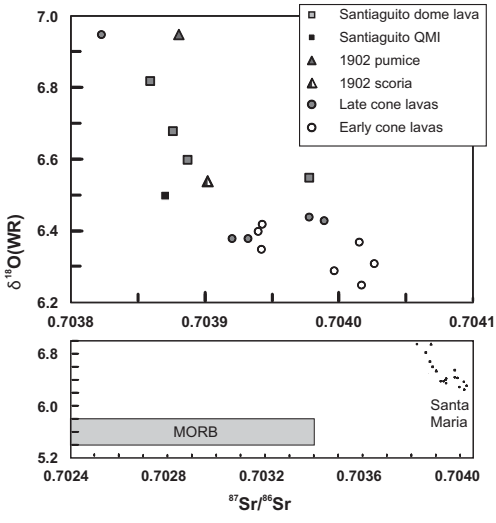

Fig. 4. Plot of $\delta^{18}O$(WR) v.$^{87}Sr/^{86}Sr$ for the Santa María cone lavas, 1902 dacite pumice and basaltic andesite scoria and Santiaguito dacite dome lavas and their quenched mafic inclusions (QMI). The lower panel shows these data relative to the range in mid-ocean ridge basalt (MORB; from data in Eiler 2001; Hofmann & Hart 1978; Cohen & O'Nions 1982).

pairs because they were encased within larger host phenocrysts. Using the two-oxide data, we take the temperature of the dacite, 880 °C, and 1020 °C of the scoria (using the three highest temperature pairs in Table 4) as our best estimates of pre-eruptive storage conditions for the compositionally zoned magma.

Plagioclase zoning and melt inclusions in 1902 dacite and scoria

The 450 plagioclase crystals imaged and analysed by EMPA display several patterns of zoning, but by far the most abundant are andesine (An_{44-36}) that include one or more irregularly sculpted resorption surfaces characterized by an abrupt rimward increase of 1020 mol% anorthite. About 80% of crystals in the dacite pumice and 70% in the basaltic andesite scoria contain more than one resorption surface, several contain as many as five of these 'saw-tooth' zones which are common in mixed or mingled calc-alkaline magmas (e.g. Singer *et al.* 1995; Humphreys *et al.* 2006). Trace element profiles show that about half of the anorthite 'spikes' are accompanied by significant changes in FeO, TiO_2, K_2O, MgO, MnO, Ba, and Sr (Fig. 8). Mantles of these phenocrysts – the outermost 10–30% of the radial distance – are not disturbed by resorption surfaces, and commonly contain low-frequency, low-amplitude oscillatory zoning, or are homogenous. About 15% of phenocrysts in the scoria are very calcic, weakly zoned (An_{93-82}), and free of resorption surfaces.

Table 3. *U–Th isotope results for Santiaguito dacite lavas and 1902 tephra*

Sample	Material	($^{230}Th/^{232}Th$)	2σ	($^{238}U/^{232}Th$)	2σ	U ppm	Th ppm
Santiaguito dome lavas (post-1902)							
SM-07-03	lava wr	1.167	0.007	1.262	0.008	0.914	2.196
SM-07-04	lava wr	1.166	0.007	1.258	0.008	0.871	2.101
SM-07-04i	inclusion wr	1.141	0.007	1.247	0.007	0.560	1.362
SM-07-06	lava wr	1.162	0.007	1.264	0.008	0.905	2.172
SM-07-06i	inclusion wr	1.138	0.007	1.256	0.008	0.551	1.330
SG-05-02	lava wr	1.172	0.007	1.258	0.008	0.882	2.127
SG-05-01	lava wr	1.174	0.007	1.279	0.008	0.954	2.261
	amphibole	1.200	0.007	1.659	0.010	0.374	0.206
	magnetite	1.172	0.007	1.375	0.008	0.561	0.256
	gmass	1.165	0.005	1.276	0.005	1.133	2.693
1902 eruption products							
SM-07-09B	wr pumice	1.155	0.007	1.277	0.008	1.054	2.503
	glass	1.182	0.005	1.276	0.005	1.304	3.102
	opx	1.204	0.013	2.541	0.015	0.178	0.213
	magnetite	1.185	0.007	1.421	0.009	0.182	0.389
SM-07-09E	wr scoria	1.143	0.007	1.193	0.007	0.559	1.420
SM-07-09F	wr lithic fragment	0.886	0.005	0.890	0.005	0.447	1.523
SM-07-09H	wr lithic fragment	0.888	0.005	0.880	0.005	0.700	2.412

Abbreviations: wr, whole rock; opx, orthopyroxene; gmass, groundmass.
The whole rock data from lavas and bulk tephra were originally reported in Jicha *et al.* (2010). They are listed here to provide context for the isotope compositions of minerals and lithic fragments.

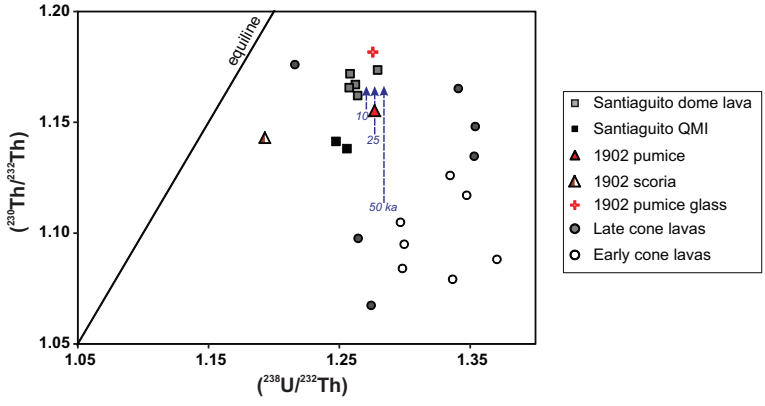

Fig. 5. Plot of ($^{238}U/^{232}Th$) and ($^{230}Th/^{232}Th$) activity ratios for basaltic andesite cone forming lavas of Santa María volcano, 1902 dacite pumice and basaltic andesite scoria, and Santiaguito dacite dome lavas and their quenched mafic inclusions (QMI). The dashed arrows indicate 10, 25 and 50 kyr of closed-system ingrowth of ^{230}Th via radioactive decay.

Approximately one-third of plagioclase crystals in the 1902 dacite pumice and one-fifth of those in the scoria contain optically clear melt inclusions. The anorthite variations and oscillatory zoning in the crystals that host these melt inclusions are similar, regardless of whether they are found in the dacite or the scoria. The melt inclusions are typically ovoid, up to 50 μm across, are commonly located along resorption surfaces, but can also be found in the cores and, less commonly, the mantles of crystals (Fig. 8). The inclusions range from dacite to high silica rhyolite with between 69 and 79 wt%, SiO_2 (anhydrous) and 1.5–3.5% K_2O (Fig. 9a). Interestingly, the melt inclusions in the dacite pumice overlap the composition of the rhyodacitic glass separated from the bulk pumice, whereas those in plagioclase from the scoria extend to significantly higher SiO_2 and K_2O contents (Fig. 9a).

The H_2O contents of 20 plagioclase-hosted melt inclusions in the dacite pumice determined by SIMS are between 1.4 and 6.9 wt% (Table 6) and in general H_2O declines as K_2O increases from about 2 to 3 wt% (Fig. 9b). Given that typical intermediate composition arc magmas contain very low amounts of dissolved CO_2 (e.g. below 400 ppm; Bacon *et al.* 1992; Wallace & Gerlach 1994; Saito *et al.* 2001; Roman *et al.* 2006), we assume that the volatile budget in the plagioclase-hosted melt inclusions in the 1902 dacite pumice is 100% H_2O. Accordingly, the pressure at which the melt inclusions were trapped was calculated using the program VolatileCalc (Newman & Lowenstern 2002) indicating minimum values for crystallization of the plagioclase between 170 and 15 MPa, corresponding to depths of about 5–1 km, or greater (Fig. 9c).

Discussion

Deep origin of dacite during volcanic repose

The decline in $^{87}Sr/^{86}Sr$, rise in $^{143}Nd/^{144}Nd$, and drop in the degree of U-excess during *c.* 75 kyr of mafic cone-building volcanism (Figs 3 & 5), led Jicha *et al.* (2010) and Singer *et al.* (2011) to infer that during this period several batches of mantle-derived basalt cooled, crystallized, partially melted lower crustal rocks that include a MORB-like component, and that blending of these partial melts with the basalt created hybrid basaltic andesite magmas. In contrast to Heydolph *et al.* (2012), who propose assimilation of mantle pyroxenite, Singer *et al.* (2011) interpret the 'old' $^{207}Pb/^{204}Pb$ ratios of the cone-forming mafic lavas to reflect fluid derived from sediment subducted into the mantle wedge. A large fluid flux beneath Santa María helps to explain the exceptionally high ^{238}U-excesses (Fig. 5) and the strongly oxidized state of these magmas (Fig. 7). The Sr, Nd, Pb, O and U–Th isotope ratios of the historically-erupted dacite pumice and lava and basaltic andesite scoria and quenched mafic inclusions are similar to the youngest cone-forming basaltic andesite lavas that, according to Jicha *et al.* (2010) and Singer *et al.* (2011), reflect a greater extent of blending basalt with lower crustal partial melts than do earlier erupted cone lavas owing to the sustained and repeated flux of basalt that progressively heated the lower crust. Development of a MASH-like zone at the base of the crust beneath Santa María was long ago proposed by Rose (1987*a*) on the basis of major element and sparse trace element data that suggested replenishment of a basaltic

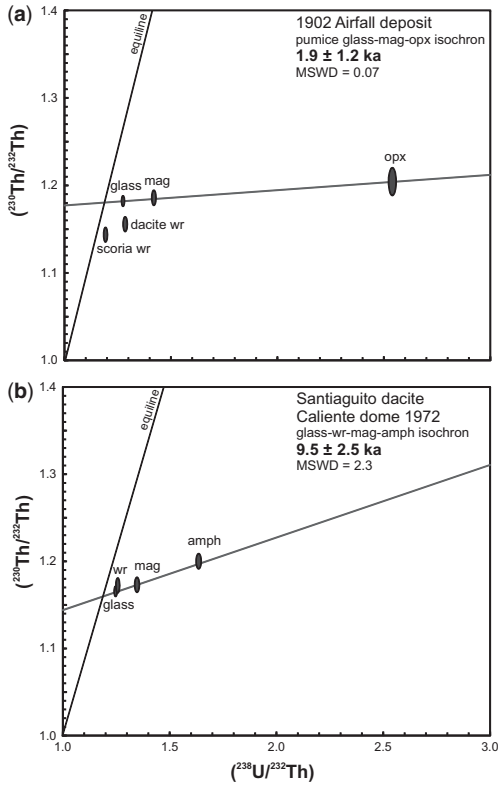

Fig. 6. Plots of ($^{238}U/^{232}Th$) and ($^{230}Th/^{232}Th$) activity ratios for: (**a**) phases from the 1902 airfall deposit including whole rock (wr) dacite pumice and glass, magnetite (mag) and orthopyroxene (opx) separated from the pumice, and whole rock scoria. The glass, magnetite and orthopyroxene yield an internal isochron of 1.9 ± 1.2 ka; (**b**) phases from the 1972 AD Caliente dacite flow, including whole rock, glass, magnetite and amphibole. These phases define an internal isochron of 9.5 ± 2.5 ka.

reservoir system in which magmas fractionally crystallized to a greater extent during the last phase of cone-growth. The similarity between the major, trace element and isotopic composition of the 1902 scoria and the last-erupted cone lavas dated between 35 and 25 ka (e.g. Figs 3 & 10) strongly argues that the historically-erupted basaltic andesite underwent similar processing in the deep crust. Rose (1987*a*) hypothesized that as the cone grew larger, the crustal column increased in thickness, thereby retarding the ability of the hybrid basaltic andesite magma to ascend to the surface.

The $^{40}Ar/^{39}Ar$ chronology of cone-building, in parallel with new trace element and isotopic data from both the composite cone (Escobar-Wolf *et al.* 2010; Singer *et al.* 2011) and now the historically-erupted dacites, enable us to further evaluate the Rose (1987*a*) hypothesis and document a major shift in processes that took place below the volcano. The $^{40}Ar/^{39}Ar$ geochronology indicates that the final, rapid pulse of cone-growth, fuelled by eruptions of hybrid basaltic andesite magma, ceased by 25 ka. We propose that at 25 ka the basaltic andesite magma began to pond deep within the crust, and having either exhausted the supply of readily fusible phases in the crustal wall rocks, or by becoming insulated from these crustal rocks as rinds or envelopes of partly solidified crystal-rich mush formed along the periphery of the MASH zone, or both, it cooled slowly such that fractional crystallization occurred without significant assimilation.

Modelling of four trace elements: K, Rb, Dy and Yb, using the EC-RAFC algorithm of Bohrson & Spera (2007), helps quantify key aspects of how basaltic andesite fractionally crystallized to form the 1902 dacite and illustrates that this behaviour contrasts sharply with that of the earlier period of open-system crystallization, melting and assimilation that affected cone-forming lavas. We chose one of the youngest cone-forming basaltic andesite lavas, sample SM-07-01 from the 3772 m summit of Santa María volcano (Singer *et al.* 2011) as a parental composition with 9681 ppm K, 22.3 ppm Rb, 3.62 ppm Dy and 2.11 ppm Yb. The liquidus temperature of this parent magma was set at 1020 °C based on two-oxide thermometry of the remarkably similar scoria in the 1902 airfall deposit (Fig. 7). The equilibration temperature of the modelled daughter magma was set at 880 °C, based also on two-oxide thermometry of the 1902 dacite pumice. A solidus temperature for hydrous hornblende dacite at lower crustal pressure was estimated at 725 °C based on experiments of Conrad *et al.* (1988). Heat capacities of the magma and wallrock are identical to those used by Singer *et al.* (2011) and recommended by Bohrson & Spera (2007) and the initial temperature of the wallrock was assumed to be 775 °C. Given these boundary conditions, the 140 °C drop in temperature from 1020 to 880 °C results in 43 wt% of the basaltic andesite parent magma crystallizing to form cumulate solids. The bulk distribution coefficients that best predict the concentrations of K, Rb, Dy and Yb in the residual melt are 0.09, 0.005, 1.75 and 1.35, respectively, consistent with fractionation of a plagioclase + hornblende + pyroxene + magnetite cumulate (Fig. 10; Davidson *et al.* 2007).

The O isotope data are consistent with the modelling presented by Singer *et al.* (2011) wherein the cone-forming basaltic andesite lavas reflect evolution of a deep crustal reservoir through both recharge with basalt and increasing extents of assimilation of a MORB-like component that, relative to the fluid-modified mantle wedge below

Table 4. *Magnetite and ilmenite compositions and T–fO_2 estimates from 1902 tephra calculated using Ghiorso & Sack (1991)*

	Pairs in dacite pumice block SM-07-09G																		Pairs in basaltic andesite scoria SM-07-09E							
	mag 1	ilm 1	mag 2	ilm 2	mag 3	ilm 3	mag 4	ilm 4	mag 5	ilm 5	mag 6	ilm 6	mag 7	ilm 7	mag 8	ilm 8	mag 9	ilm 9	mag 1	ilm 1	mag 2	ilm 2	mag 3	ilm 3	mag 4	ilm 4
SiO_2	0.08	0.05	0.06	0.04	0.07	0.02	0.07	0.03	0.09	0.05	0.07	0.08	0.06	0.05	0.07	0.07	0.07	0.03	0.10	0.10	0.06	0.02	0.10	0.08	0.06	0.07
TiO_2	5.68	35.84	5.79	36.50	5.59	35.94	5.80	36.51	5.75	36.42	5.52	35.82	5.65	36.49	5.63	35.60	5.63	35.13	8.07	35.34	6.75	36.14	8.09	35.85	5.92	34.69
Al_2O_3	2.41	0.31	2.31	0.33	2.11	0.30	2.29	0.35	2.28	0.33	2.43	0.35	2.45	0.32	2.26	0.34	2.26	0.04	1.68	0.12	2.62	0.42	1.70	0.37	1.96	0.12
FeO	82.34	54.17	84.17	54.42	84.40	54.10	82.24	54.69	82.02	55.41	82.32	55.51	82.63	54.30	81.32	54.44	81.32	55.12	79.15	53.04	82.48	56.16	79.20	54.49	84.00	54.80
MnO	0.89	1.47	0.93	1.34	0.92	1.41	0.94	1.30	1.03	1.27	1.00	1.02	0.85	1.49	0.90	1.16	0.90	1.19	0.90	1.03	0.79	0.60	0.90	1.02	1.04	0.61
MgO	1.63	2.28	1.51	2.20	1.49	2.27	1.57	2.22	1.54	2.17	1.36	1.76	1.62	2.21	1.50	2.17	1.50	2.20	1.73	3.48	1.83	2.53	1.84	1.74	1.57	1.96
CaO	0.01	0.02	0.02	0.02	0.00	0.02	0.03	0.05	0.01	0.00	0.03	0.03	0.01	0.03	0.01	0.03	0.01	0.05	0.09	0.21	0.00	0.02	0.11	0.02	0.02	0.08
Cr_2O_3	0.02	0.01	0.00	0.00	0.00	0.02	0.03	0.01	0.02	0.02	0.01	0.01	0.00	0.00	0.03	0.00	0.03	0.00	0.03	0.01	0.06	0.01	0.03	0.01	0.03	0.04
ZnO	0.18	0.12	0.15	0.06	0.15	0.07	0.15	0.04	0.18	0.09	0.19	0.11	0.16	0.14	0.20	0.05	0.15	0.08	0.17	0.07	0.06	0.05	0.19	0.12	0.13	0.06
V_2O_3	0.10	0.02	0.14	0.00	0.15	0.00	0.09	0.02	0.02	0.03	0.25	0.78	0.18	0.22	0.28	0.32	0.20	0.01	0.16	0.06	0.26	0.00	0.18	0.78	0.00	0.00
Total	93.35	94.28	95.08	94.91	94.89	94.15	93.21	95.21	92.94	95.79	93.18	95.47	93.61	95.25	92.20	94.18	92.07	93.85	92.07	93.47	94.91	95.94	92.34	94.48	94.73	92.43
XIlm		0.662		0.674		0.665		0.670		0.667		0.668		0.673		0.674		0.677		0.633		0.658		0.674		0.670
XUsp	0.158		0.158		0.152		0.161		0.159		0.158		0.158		0.156		0.156		0.232		0.190		0.233		0.163	
T (°C)	877		869		864		876		876		864		871		878		876		1009		929		1009		1039	
log fO_2	−10.35		−10.54		−10.60		−10.41		−10.39		−10.59		−10.49		−10.35		−10.41		−8.47		−9.51		−8.39		−7.89	

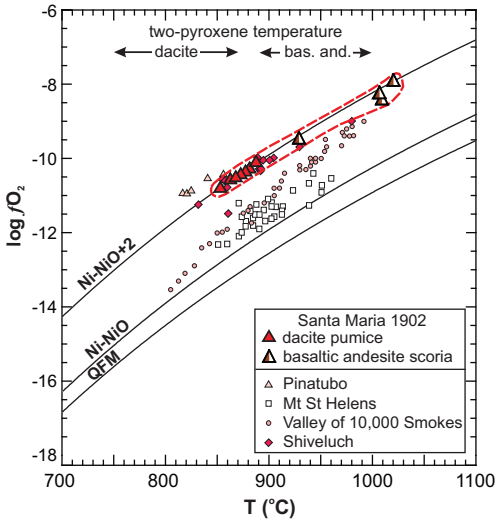

Fig. 7. Calculated equilibration temperature and oxygen fugacity (fO_2) for Fe–Ti oxide pairs. Each pair of grains is located within a single host phenocryst in the 1902 dacite pumice or scoria. The range of temperature estimates for co-existing pyroxenes in the 1902 dacite and scoria are indicated (representative data from Table 5). For comparison, Fe–Ti results from Pinatubo (Hattori 1993), Mt St Helens, Shiveluch (Blundy *et al.* 2006) and the Valley of Ten Thousand Smokes (Hildreth 1983) are illustrated.

Santa María, is characterized by lower $^{87}Sr/^{86}Sr$ ratios and higher $\delta^{18}O$ values (Fig. 4).

The O isotope data are also consistent with a closed-system crystallization origin of the dacites from basaltic andesite magma left-over from the cone-building period. It is well known that extensive high temperature crystallization of calc-alkaline magmas has little effect, perhaps increasing by a few tenths permil, on $\delta^{18}O$ of derivative magmas (Matsuhisa 1979; Singer *et al.* 1992). Specifically, crystal fractionation of parent magmas similar to the cone-forming lavas at Santa María with between 50 and 54% SiO_2 and $\delta^{18}O$ values of between 6.50 and 6.95‰ could produce the historically erupted dacites. Conspicuously, the youngest cone-forming basaltic andesite lava that we have measured (sample SM-07-01 that was used as a parent magma in the fractional crystallization model) has a $\delta^{18}O$ value identical to the 1902 dacite and thus represents a potential parent magma for this dacite (Fig. 3). If assimilation has also contributed to the origin of the dacites, the assimilant must have a $\delta^{18}O$(WR) value similar to that of the late cone-forming lavas.

The $^{238}U/^{230}Th$ isochron of 1.9 ± 1.2 ka defined by glass, magnetite and orthopyroxene in the 1902 dacite pumice (Fig. 6a) implies that crystals carried to the surface in this magma began to form very shortly before the eruption. That the whole rock sample of 1902 dacite pumice falls below the isochron may reflect mixing between the basaltic andesite, which plots well below the isochron, and the bulk dacite, that lies between the basaltic andesite and the isochron (Fig. 6a). Mixing of the basaltic andesite with the dacite is recorded in detail in the zoning of plagioclase phenocrysts in both of these magmas (Fig. 9) that will be discussed below. More surprising is the 9.5 ± 2.5 ka $^{238}U/^{230}Th$ isochron defined by glass, magnetite, amphibole and bulk material from the 1972 lava flow on the north flank of the Caliente dacite dome (Figs 2 & 6b). From this isochron, we infer that portions of the dacite magma which now comprise the Santiaguito dome complex that grew via effusive and mildly explosive activity in the decades following the explosive onset of silicic volcanism at Santa María in 1902, began to crystallize several thousand years prior to the 1902 eruption. In this scenario, deeper, occluded reaches of the dacite magma body, perhaps including crystal-rich zones near the cooler, more viscous, periphery of the silicic reservoir, had begun to solidify no later than 10 kyr prior to the Plinian eruption of 1902, but were unable to erupt until decades after the eruption in 1902 of the more silica- and H_2O-rich melt layer that capped the system.

The volume of dacite erupted explosively in 1902 is estimated at 8.5 km^3 dense rock equivalent (Williams & Self 1982). If our model is correct, the minimum volume of basaltic andesite parent magma required to create the 1902 dacite is about 20 km^3. Notably, this is well within the 40–67 km^3 of magma estimated to have fuelled the preceding growth of the 8 km^3 cone of basaltic andesite that comprises Santa María volcano, based on EC-RAFC modelling that accounts for recharging of the system with mantle-derived magma, assimilation of partially melted crust, and fractional crystallization (Fig. 10c; Singer *et al.* 2011). Using the thermal model of Hawkesworth *et al.* (2000) and a cooling time of 25 kyr suggests that a 20 km^3 mass of basaltic andesite which drops 140 °C and crystallizes 43% would generate a power output of about 25 MW, which is perhaps an order of magnitude lower than power generated during the preceding period of open-system behaviour during the later period of cone growth. The correspondingly modest and protracted release of heat during 25 kyr of cooling in the deep crust may also explain why evidence that partial melting and assimilation were important in creating a large volume of dacite is absent. If the 9.5 ± 2.5ka $^{238}U/^{230}Th$ isochron from the 1972 Caliente flow is

Table 5. *Representative pairs of pyroxene core compositions with T estimates using equations 36 and 37 from Putirka (2008)*

	1902 dacite pumice SM-07-09G											1902 basaltic andesite scoria SM-07-09E						
Clinopyroxenes																		
SiO_2	51.76	52.82	53.13	52.69	52.81	51.14	52.56	53.25	53.31	52.99	52.38	51.43	50.05	49.13	53.45	50.64	49.13	52.44
TiO_2	0.32	0.38	0.15	0.17	0.22	0.27	0.27	0.12	0.11	0.16	0.26	0.62	0.80	0.84	0.17	0.73	0.84	0.54
Al_2O_3	1.51	2.04	0.87	1.23	1.17	3.75	1.77	0.93	0.94	1.05	1.36	3.54	4.14	4.92	0.95	3.75	4.92	3.63
FeO	10.91	10.51	10.11	11.18	11.82	10.78	11.01	11.70	10.55	11.14	11.71	8.79	8.95	9.51	9.62	8.27	9.51	8.80
MnO	0.37	0.28	0.46	0.43	0.32	0.32	0.31	0.44	0.32	0.55	0.32	0.21	0.24	0.26	0.45	0.21	0.26	0.25
MgO	11.93	14.01	13.08	12.12	12.21	11.40	12.01	12.30	12.55	11.90	12.13	14.93	14.20	14.21	13.57	14.38	14.21	15.55
CaO	21.68	20.12	21.38	21.85	21.52	21.53	22.04	21.29	22.20	21.83	21.39	19.27	20.10	19.21	21.83	20.91	19.21	18.97
Na_2O	0.32	0.31	0.36	0.28	0.31	0.33	0.39	0.23	0.23	0.39	0.30	0.49	0.45	0.44	0.31	0.35	0.44	0.48
K_2O	0.03	0.01	0.01	0.00	0.00	0.18	0.00	0.01	0.01	0.00	0.01	0.00	0.00	0.00	0.01	0.01	0.00	0.00
Cr_2O_3	0.02	0.01	0.00	0.02	0.01	0.05	0.02	0.04	0.01	0.01	0.02	0.01	0.03	0.06	0.02	0.01	0.06	0.06
Total	98.86	100.49	99.54	99.96	100.40	99.76	100.38	100.31	100.24	100.02	99.88	99.29	98.96	98.58	100.38	99.26	98.58	100.71
Orthopyroxenes																		
SiO_2	53.82	53.77	54.04	53.93	53.57	53.87	53.93	53.58	53.73	53.27	53.52	53.36	53.86	53.68	52.94	53.55	53.90	53.78
TiO_2	0.13	0.10	0.12	0.11	0.19	0.11	0.11	0.03	0.12	0.12	0.13	0.36	0.22	0.11	0.11	0.24	0.16	0.19
Al_2O_3	1.01	1.01	0.96	0.92	0.89	1.00	0.96	1.03	1.09	0.96	1.02	2.38	1.58	1.16	0.56	2.07	0.64	0.70
FeO	18.78	18.38	18.38	18.45	21.84	18.02	18.53	18.58	18.47	18.26	18.80	15.95	16.48	18.24	23.76	16.31	19.53	19.62
MnO	2.64	1.92	2.50	2.18	0.59	1.86	1.92	2.50	1.91	1.91	1.84	0.52	0.59	2.68	0.87	0.40	1.02	0.92
MgO	23.16	23.51	23.06	23.41	21.88	23.45	23.51	23.17	23.47	23.43	23.39	24.96	25.12	23.31	20.42	25.31	23.19	23.08
CaO	0.43	0.70	0.44	0.52	0.65	0.69	0.69	0.44	0.66	0.70	0.61	1.90	1.70	0.37	0.96	1.45	0.96	1.13
Na_2O	0.02	0.01	0.00	0.00	0.00	0.03	0.03	0.01	0.00	0.02	0.02	0.04	0.04	0.03	0.02	0.03	0.01	0.00
K_2O	0.01	0.02	0.00	0.00	0.00	0.01	0.00	0.01	0.00	0.00	0.00	0.00	0.00	0.00	0.00	0.00	0.00	0.01
Cr_2O_3	0.02	0.02	0.00	0.01	0.01	0.00	0.01	0.01	0.01	0.00	0.00	0.03	0.02	0.00	0.00	0.01	0.00	0.01
Total	100.02	99.44	99.51	99.53	99.63	99.04	99.70	99.34	99.48	98.67	99.33	99.49	99.62	99.58	99.64	99.36	99.42	99.44
K_D (Cpx/Opx)	1.13	0.96	0.97	1.17	0.97	1.23	1.16	1.19	1.07	1.20	1.20	0.92	0.96	0.86	0.89	0.82	0.80	0.67
T(°C) eq. 36	737	855	761	759	896	788	767	779	766	761	805	997	972	860	961	951	958	964
T(°C) eq. 37	724	883	761	739	850	775	738	779	739	730	786	1002	966	927	940	965	999	1022
T (°C) ave.	731	869	761	749	873	781	752	779	753	746	795	1000	969	893	951	958	978	993

Oxides in wt%.

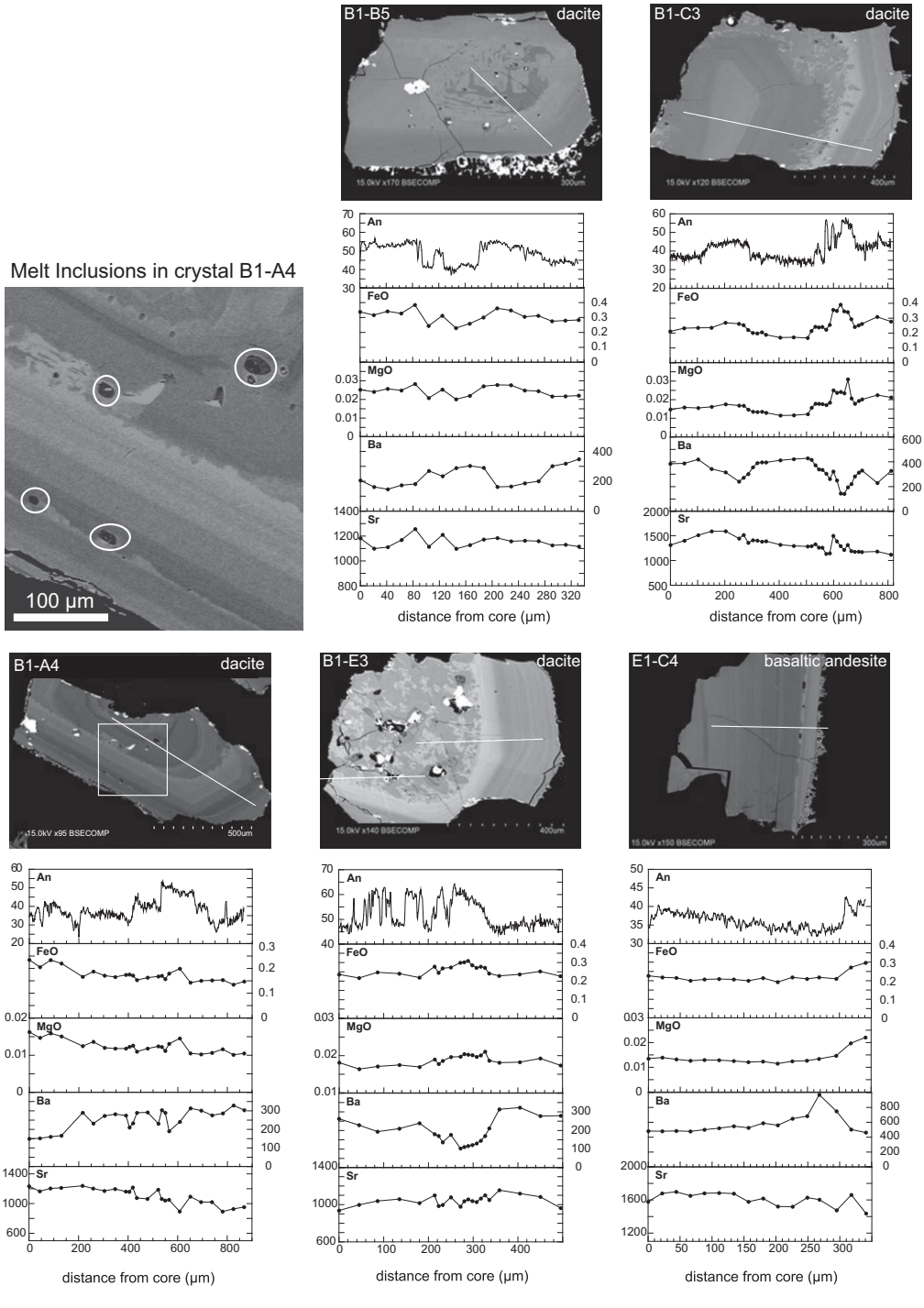

Fig. 8. Representative illustrations of zoning and melt inclusions in plagioclase revealed by backscattered electron images. Core-to-rim profiles of measured anorthite content determined by wavelength dispersive electron probe microanalysis, and FeO, MgO, Ba and Sr contents determined by secondary ion mass spectrometry. The box in the lower left panel with a backscattered electron image is enlarged above to show four melt inclusions typical of those measured for H_2O contents. See text for discussion.

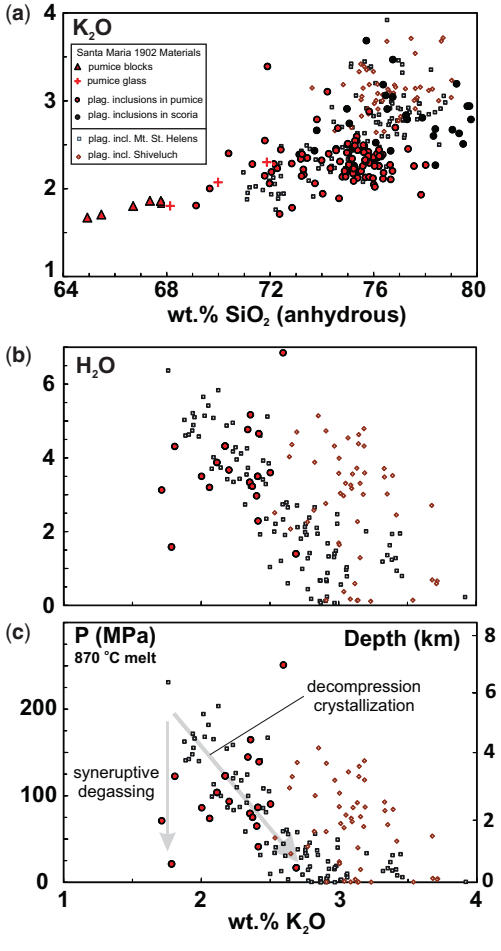

Fig. 9. Compositions of plagioclase-hosted melt inclusions. (**a**) K_2O v. SiO_2 plot shows that inclusions in 1902 dacite pumice overlap the composition of bulk glass separated from pumice blocks and that together inclusions in the pumice and scoria span a range of composition similar to that of phenocryst-hosted melt inclusions from Mt St Helens and Shiveluch dacite and andesite (data from Blundy *et al.* 2006). Inclusion compositions obtained by electron probe microanalysis, dacite pumice and glass by X-ray fluorescence. (**b**) H_2O (wt%) v. K_2O plot for 20 melt inclusions in 1902 dacite pumice. The vast majority of inclusions show a decline in H_2O with increasing SiO_2 comparable to the inclusions in Mt St Helens dacite (data from Blundy *et al.* 2006). (**c**) Interpretation of the variation in melt inclusion compositions (see text for details).

representative of when a large portion of the dacite began to crystallize, the 25 MW estimate of power output is a maximum. Alternatively, it seems likely that portions of the dacite magma may have crystallized at various times during the past 25 kyr, depending on where–within the plexus of mushy-to-molten environments of the deep crustal MASH zone–they began to cool.

An additional clue that may bear on the duration of the closed-system fractional crystallization process is the U–Th isotope composition of the quenched basaltic andesite inclusions found in the 1972 El Brujo dacite dome lava and the 1939 La Mitad dacite dome lava (Samples SM-07-04i and -06i; Tables 1 and 3). The two inclusions have nearly identical ($^{230}Th/^{232}Th$) and ($^{238}U/^{232}Th$) activity ratios of 1.14 and 1.25, respectively, despite being erupted 33 years apart and from nearly opposite ends, about 2 km apart, of the Santiaguito dome complex (Fig. 2). Their ($^{238}U/^{232}Th$) activity ratio is slightly lower than that of the 1902 dacite pumice and Santiaguito dacite dome lavas, consistent with fractionation of amphibole + clinopyoxene in which $D_{Th} > D_U$ and generation of a slight ^{238}U excess is to be expected (Brenan *et al.* 1995). Moreover, the ($^{230}Th/^{232}Th$) ratio is significantly lower than the dacites by an amount equivalent to 25 kyr of closed-system ingrowth of ^{230}Th (Fig. 5). These two inclusions are remarkably similar, not only in U–Th isotope composition, but also in major and most trace element concentrations, to the basaltic andesite lava, SM-07-01, used as a parent magma in the fractional crystallization model illustrated in Figure 10.

New fuel to the fire: the 1902 basaltic andesite and shallow processes

The Sr, Nd and Pb isotope ratios of the 1902 basaltic andesite scoria are, on average, slightly different than the average ratio of the 1902 dacite pumice or glass (Fig. 3). However, the scoria is lower in $\delta^{18}O$ than the dacite. Moreover, the scoria has a U–Th isotope composition that is slightly lower in ($^{230}Th/^{232}Th$) than the 1902 dacite pumice, but significantly lower in ($^{238}U/^{232}Th$) than either the 1902 pumice or the basaltic andesite inclusions in the 1939 and 1972 Santiaguito dacite dome lavas (Figs 5 & 6a). Collectively, these observations indicate that the basaltic andesite scoria produced mainly at the end of the 1902 Plinian eruption is not directly related to the much larger mass of dacite erupted at the onset. Instead, we propose that this basaltic andesite represents an influx of new magma into the MASH zone that, shortly prior to the 1902 eruption, spread out beneath the dacite magma, but was prohibited from mixing across the interface by the contrasts in both density and viscosity of the two magmas. The basaltic andesite supplied heat and perhaps volatiles via diffusion across the interface to the dacite, but, as two-oxide thermometry shows, thermal equilibration, and thus extensive

Table 6. *Representative plagioclase-hosted melt inclusion compositions*

1902 Dacite pumice sample SM-07-09G																			
Crystal#	**B1-A4-1**	**B1-A4-2**	**B1-B3-1**	**B1-B3-2**	**B1-B5-2**	**B1-B5-3**	**B1-B5-4**	**B1-B5-5**	**B1-B5-7**	**B1-B7-5**	**B1-C3-1**	**B1-C3-2**	**B1-C3-3**	**B1-C3-4**	**B1-C3-5**	**B1-E3-1**	**B1-E3-2**	**B1-E3-3**	**B1-E3-4**
Position	mantle	rim	rim	rim	core	core	core	core	mantle	mantle	rim	rim	rim	rim	rim	core	core	core	core
SiO_2	70.95	70.82	71.05	69.90	67.15	66.41	68.37	66.56	69.98	70.74	68.23	71.86	64.54	69.58	69.97	72.23	73.53	72.72	71.17
Al_2O_3	13.74	13.45	13.84	13.50	16.61	14.31	16.19	15.28	14.23	13.64	14.93	15.68	17.14	13.07	13.29	14.26	14.00	13.91	13.50
TiO_2	0.13	0.19	0.24	0.29	0.16	0.27	0.32	0.06	0.25	0.23	0.14	0.28	0.11	0.07	0.16	0.28	0.35	0.23	0.20
MgO	0.37	0.40	0.41	0.37	0.72	0.65	0.75	0.77	0.58	0.44	0.41	0.33	0.36	0.49	0.44	0.44	0.41	0.41	0.46
FeO	1.14	1.03	1.46	1.39	2.25	1.83	2.22	2.18	1.82	1.44	1.16	1.24	1.25	1.47	1.45	1.46	1.30	1.58	1.50
CaO	1.44	1.32	1.64	1.60	3.00	2.47	3.06	2.64	2.02	1.53	2.34	2.87	4.03	1.61	1.46	1.62	1.80	1.73	1.70
Na_2O	2.95	2.77	3.50	2.33	4.31	4.01	1.81	4.41	4.08	3.28	3.51	4.55	4.05	2.90	3.09	3.57	4.08	4.07	3.79
K_2O	2.11	2.20	2.50	2.36	2.00	2.06	1.71	2.40	2.35	2.60	2.34	1.78	1.81	2.42	2.37	2.17	2.41	2.69	2.41
MnO	0.08	0.12	0.11	0.26	0.19	0.25	0.06	0.26	0.07	0.00	0.18	0.05	0.07	0.19	0.09	0.03	0.15	0.12	0.12
Total	92.92	92.31	94.76	91.99	96.39	92.28	94.48	94.56	95.39	93.89	93.23	98.64	93.36	91.80	92.32	96.05	98.04	97.46	94.85
H_2O 1	3.22	3.67	3.60	5.17	3.50	3.20	3.13	2.97	3.23	6.85	4.77	1.73	4.31	4.66	3.23	4.45	2.29	1.48	3.82
H_2O 2	4.53		3.60						3.45			1.44				4.19		1.32	3.18
P (MPa)	104	93	90	165	86	74	65	75	80	251	145	21	122	139	73	123	41	17	86

1902 Basaltic andesite scoria sample SM-07-09E																			
Crystal#	**E1-A10-1**	**E1-B10-1**	**E1-C4-1**	**E1-C4-2**	**E1-D9-1**	**E1-E10-1**	**E2-A3-1**	**E2-B9-1**	**E3-C3-1**	**E2-C3-2**	**E2-C9-2**	**E3-A1-1**	**E3-A1-2**	**E3-B1-1**	**E3-B8-1**	**E3-C1-1**	**E3-D8-1**	**E3-E4-1**	**E3-E6-1**
Position	rim	mantle	rim	rim	rim	core	core	mantle	rim	rim	rim	rim	rim	rim	mantle	mantle	rim	mantle	mantle
SiO_2	75.52	74.71	73.13	72.62	71.48	72.49	74.00	72.80	71.61	73.88	73.65	71.40	70.27	72.77	74.99	75.35	74.44	73.85	74.70
Al_2O_3	13.13	12.27	11.13	11.76	11.38	11.79	12.40	12.38	13.41	12.34	11.92	10.77	11.41	11.89	12.20	11.03	10.54	11.01	13.45
TiO_2	0.19	0.13	0.28	0.26	0.29	0.28	0.25	0.25	0.26	0.22	0.36	0.34	0.41	0.12	0.10	0.17	0.11	0.26	0.22
MgO	0.28	0.25	0.23	0.27	0.87	0.29	0.14	0.32	0.04	0.04	0.80	0.68	1.00	0.17	0.08	0.11	0.31	0.40	0.36
FeO	1.13	0.92	1.29	1.17	3.69	1.27	0.51	0.90	0.29	0.26	1.96	3.87	4.78	0.35	0.28	0.26	1.67	1.27	1.60
CaO	0.88	0.97	0.70	0.71	0.74	0.93	1.42	0.99	1.36	1.09	0.69	0.64	0.53	0.97	0.83	0.65	0.69	0.63	0.82
Na_2O	4.57	3.87	2.14	2.15	2.04	1.99	3.18	1.46	2.12	1.11	3.87	1.87	2.41	2.09	2.22	1.58	1.97	1.86	3.82
K_2O	3.06	2.81	2.94	2.63	2.91	2.67	2.60	2.51	2.27	4.47	3.19	3.47	2.91	2.94	2.33	3.14	2.93	2.72	3.69
MnO	0.00	0.00	0.00	0.00	0.00	0.00	0.00	0.00	0.00	0.00	0.00	0.00	0.00	0.00	0.00	0.00	0.00	0.00	0.00
Total	98.77	95.93	91.84	91.57	93.40	91.71	94.49	91.62	91.35	93.42	96.44	93.04	93.73	91.30	93.03	92.29	92.66	91.99	98.66

Oxides in wt%. H_2O determined by SIMS. Minimum pressure calculated using Newman & Lowenstern (2002). Where two independent H_2O analyses (H_2O 1 & 2) are reported from 6 of the 19 inclusions in the dacite pumice, the average minimum pressure is calculated.

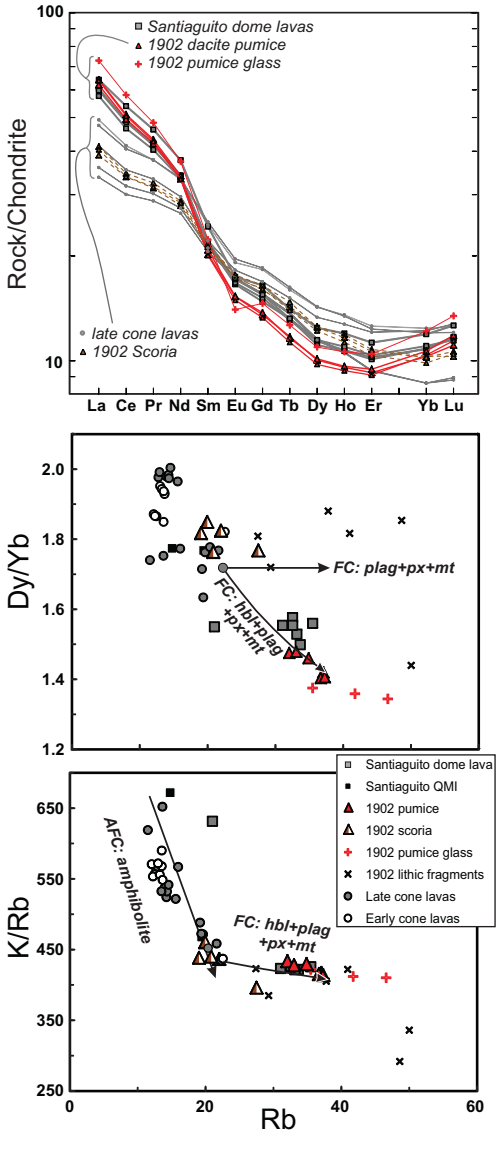

Fig. 10. Trace element variation in Santa María dacites. In upper panel chondrite-normalized rare earth element (REE) contents indicate that dacites are depleted in middle to heavy REE relative to cone-forming and 1902 basaltic andesite compositions (normalizing values from Sun & McDonough 1989). The process diagrams of Dy/Yb and K/Rb v. Rb in the middle and lower panels illustrate fractional crystallization models discussed in the text.

chemical mixing of the two magmas, did not take place (Sparks & Marshall 1986). However, the resulting increase in buoyancy, even if small, may have rapidly promoted convection within the dacite and exsolution of H_2O across the upper part of the dacite magma cap (Snyder 2000). In turn, exsolution and vesiculation could have initiated the ascent of magma that led to the Plinian eruption.

Plagioclase zoning and the compositions of melt inclusions provide additional clues about processes that attended the latest stages of evolution of the two magmas that erupted in 1902. The abrupt, large amplitude reversals in plagioclase zoning that occur rimward of resorption surfaces and are commonly accompanied by increases in FeO, MgO, and Sr (Fig. 8) in phenocrysts contained in both the 1902 dacite pumice and scoria, argue that these two magmas mingled physically and that some limited chemical mixing had also begun to take place (e.g. Singer *et al.* 1995; Humphreys *et al.* 2006). The remarkable similarity in zoning–including multiple reversals of composition–within the majority of phenocrysts in the two magmas, together with the overlapping composition of melt inclusions trapped in these phenocrysts (Fig. 9a), imply that many plagioclase crystals were exchanged back-and-forth between rhyolitic melt and basaltic andesite magma.

The co-variation of K_2O and SiO_2 in the plagioclase-hosted melt inclusions (Fig. 9a) is consistent with fractional crystallization of the 1902 dacite magma to produce rhyodacite to high-silica rhyolite melt compositions. Moreover, the drop in H_2O with increasing K_2O recorded by the vast majority of these melt inclusions is remarkably similar to the behaviour recorded by plagioclase and amphibole-hosted melt inclusions in the dacite pumice and lava erupted during May to October, 1980 at Mt St Helens (Fig. 9b; Blundy & Cashman 2005). The drop in H_2O with increasing K_2O is also paralleled by andesite pumice erupted between 2001 and 2004 at Shiveluch volcano, Kamchatka (Blundy *et al.* 2006). Blundy & Cashman (2005) and Blundy *et al.* (2006) have proposed that this co-variation reflects decompression-driven crystallization of the melt under water-saturated conditions at both Mt St Helens and Shiveluch volcanoes (Fig. 9c). The co-variation of H_2O and K_2O in the 1902 Santa María dacite strongly suggests that rapid decompression-driven crystallization of plagioclase from pressures of at least 180 MPa or >5 km depth occurred *en route* to the surface such that few inclusions experienced syneruptive degassing and most record evolution of residual high silica rhyolite melt (Fig. 9c). If correct, this conclusion suggests that the model of Blundy & Cashman (2005) may apply widely to dacitic magma that erupts explosively in subduction zones around the world.

The exchange of plagioclase crystals between the thermally and chemically contrasting melts led

to the repeated reversals in zoning during mingling and mixing of the two magmas that occurred mainly during magma ascent. It is remarkable that the interaction of these two contrasting magmas *en route* to the surface – a complication that did not affect the Mt St Helens dacite (Blundy & Cashman 2005; Blundy *et al.* 2006) – led to complex zoning in plagioclase, but did not obliterate the signature of H_2O-saturated decompression of the silicic melts. Perhaps, more importantly, the plagioclase crystals that dominate the phenocryst modes of the 1902 dacite and scoria record mainly late-stage, shallow-level, fractional crystallization that occurred after the large body of volatile-rich dacite had accumulated during an earlier, and likely far more protracted, period of fractional crystallization deep within the crust. Thus, andesitic to dacitic magma erupted explosively at frontal arc composite volcanoes including Mt St Helens (Berlo *et al.* 2007), Shiveluch (Blundy *et al.* 2006; Humphreys *et al.* 2006), and Santa María appears to share a common two-stage crystallization history. At Santa María volcano, a 'snap-shot' recording of the early stage of fractional crystallization – corresponding to slow cooling in the deep crust – is reflected in the 9.5 ± 2.5 ka $^{238}U-^{230}Th$ isochron of the 1972 dome lava and the U–Th isotope composition of quenched mafic inclusions in the dome lavas (Figs 5 & 6b), whereas the later and more rapid decompression-driven crystallization in the conduit during magma ascent to the surface is consistent with the 1.9 ± 1.2 ka isochron from the 1902 dacite pumice (Fig. 6a).

Conclusions

Although in terms of eruptive history and magma compositions, Volcán de Santa María is relatively simple, and strongly bimodal, with 8 km^3 of basaltic andesite erupted between about 100 and 25 ka, and >9 km^3 of dacite erupted historically, generation of the highly explosive dacite was complex and took place over tens of thousands of years, mainly at depths greater than 5 km during a period of volcanic repose. During *c.* 75 kyr of cone-building, trace element and Sr–Nd–Pb–O and U–Th isotope data indicate that lower crustal heating sufficient to induce partial melting and assimilation involved several pulses of recharging mantle-derived basalt. A fundamental shift in process coincides with the termination of cone-building at 25 ka: the 1902 dacite reflects >40% fractional crystallization of plagioclase + amphibole + pyroxene + magnetite from ~20 km^3 of basaltic andesite magma left-over from cone-building that cooled slowly without assimilating significant amounts of additional crust.

Small contrasts in Sr–Nd–Pb isotope ratios, a modest contrast in $\delta^{18}O$, and a significant difference in the ($^{238}U/^{230}Th$) activity ratio between the 1902 scoria and dacite indicate that these two magmas are not strictly consanguineous, rather this basaltic andesite is likely a recent arrival in the system. A glass–whole rock–magnetite–amphibole $^{238}U-^{230}Th$ isochron of 9.5 ± 2.5 ka for a 1972 Santiaguito dacite lava suggests that deeper, occluded portions of the silicic magma body not erupted in 1902 incubated in the crust for at least 10 kyr, and perhaps longer, prior to the 1902 eruption.

Following fractional crystallization deep in the crust, the final phase of creating the 1902 dacite involved rapid decompression and crystallization of the magma *en route* to the surface, as has been proposed at other intermediate composition subduction-zone volcanoes. Importantly, the phenocrysts that grew during this late stage of fractional crystallization had little to do with the formation of the dacite itself. Instead, the composition of the dacite reflects mainly slow, hydrous crystallization of amphibole over tens of thousands of years from basaltic andesite ponded deep within the crust. Arrival of an isotopically distinct mass of basaltic andesite into this deep crustal MASH zone may have supplied heat that promoted buoyancy, convection and vesiculation within dacite that, in turn, initiated ascent and the Plinian eruption of 1902.

We thank Bill Rose, Rüdiger Escobar-Wolf and the geologists and staff of INSIVUMEH, Guatemala for guidance in the field, and John Hora for laboratory assistance. Reviews by Bill Rose and especially Simon Turner, as well as the editorial comments of Georg Zellmer, helped us clarify several issues and are much appreciated. This study was supported by NSF Grant EAR-0738007 (Singer and Jicha). The WiscSIMS ion microprobe lab is partly supported by NSF EAR (grants 0319230, 0744079, 1053466).

References

Annen, C., Blundy, J. D. & Sparks, S. J. 2006. The genesis of intermediate and silicic magmas in deep crustal hot zones. *Journal of Petrology*, **47**, 505–539.

Armstrong, J. 1988. Quantitative analysis of silicate and oxide materials: comparison of Monte Carlo, ZAF, and φ(ρz) procedures. *In*: Newbury, D. E. (ed.) *Microbeam Analyses*. San Francisco Press, San Francisco, 239–246.

Bacon, C. & Hirschmann, M. 1988. Mg/Mn partitioning as a test for equilibrium between coexisting Fe–Ti oxides. *American Mineralogist*, **73**, 57–61.

Bacon, C. R. & Lowenstern, J. B. 2005. Late Pleistocene granodiorite source for recycled zircon and phenocrysts in rhyodacite lava at Crater Lake, Oregon. *Earth and Planetary Science Letters*, **233**, 277–293.

Bacon, C., Newman, S. & Stolper, E. 1992. Water, CO_2, Cl, and F in melt inclusions in phenocrysts from three

Holocene explosive eruptions, Crater Lake, Oregon. *American Mineralogist*, **77**, 1021–1030.

BACON, C. R., SISSSON, T. W. & MAZDAB, F. K. 2007. Young cumulate complex beneath Veniaminof caldera, Aleutian arc, dated by zircon in erupted plutonic blocks. *Geology*, **35**, 491–494.

BECCALUVA, L., BELLIA, S. *ET AL.* 1995. The northwestern border of the Caribbean plate in Guatemala: new geological and petrological data on the Motagua ophiolitic belt. *Ophioliti*, **20**, 1–15.

BERLO, K., BLUNDY, J., TURNER, S. & HAWKESWORTH, C. 2007. Textural and chemical variation in plagioclase phenocrysts from the 1980 eruptions of Mount St. Helens, USA. *Contributions to Mineralogy and Petrology*, **154**, 291–308.

BLUNDY, J. D. & CASHMAN, K. 2005. Rapid decompression-driven crystallization recorded by melt inclusions from Mount St. Helens volcano. *Geology*, **33**, 793–796.

BLUNDY, J. D., CASHMAN, K. & HUMPHREYS, M. 2006. Magma heating by decompression-Driven crystallization beneath andesite volcanoes. *Nature*, **443**, 76–80.

BOHRSON, W. A. & SPERA, F. J. 2007. Energy-Constrained Recharge, Assimilation, and Fractional Crystallization (EC-RA$_x$FC): a Visual Basic computer code for calculating trace element and isotope variations of open-system magmatic systems. *Geochemistry, Geophysics, Geosystems*, **8**, 2007GC001781.

BRENAN, J. M., SHAW, H. F., RYERSON, F. J. & PHINNEY, D. L. 1995. Experimental-determination of trace-element partitioning between pargasite and a synthetic hydrous andesitic melt. *Earth and Planetary Science Letters*, **135**, 1–11, doi: http://dx.doi.org/10.1016/0012-821X(95)00139-4.

CARR, M. J. 1984. Symmetrical and segmented variation of physical and geochemical characteristics of the Central American volcanic front. *Journal of Volcanology and Geothermal Research*, **20**, 231–252.

CARR, M. J., FEIGENSON, M. D., PATINO, L. C. & WALKER, J. A. 2003. Volcanism and geochemistry in Central America: progress and problems. *In*: EILER, J. (ed.) *Inside the Subduction Factory*. American Geophysical Union, Washington, DC, 153–174.

CARR, M. J., PATINO, L. C. & FEIGENSON, M. D. 2007. Petrology and geochemistry of Lavas. *In*: BUNDSCHUH, J. & ALVARADO, G. E. (eds) *Central America: Geology, Resources, and Hazards*. Taylor & Francis, London, 565–590.

COHEN, R. S. & O'NIONS, R. K. 1982. The lead, neodymium and strontium isotopic structure of ocean ridge basalts. *Journal of Petrology*, **23**, 299–324.

CONDOMINES, M., GAUTHIER, P.-J. & SIGMARSSON, O. 2003. Timescales of magma chamber processes and dating of young volcanic rocks. *In*: BOURDON, B., HENDERSON, G. M., LUNDSTROM, C. C. & TURNER, S. P. (eds) *Uranium Series Geochemistry,* Reviews in Mineralogy and Geochemistry. Mineralogical Society of America, Washington, DC, 125–174.

CONRAD, W. K., NICHOLLS, I. A. & WALL, V. J. 1988. Water-saturated and -undersaturated melting of metaluminous and peraluminous crustal compositions at 10 kb: evidence for the origin of silicic magmas in the Taupo Volcanic Zone, New Zealand, and other occurrences. *Journal of Petrology*, **29**, 765–803.

DAVIDSON, J., TURNER, S., HANDLEY, H., MACPHERSON, C. & DOSSETO, A. 2007. An amphibole 'sponge' in arc crust. *Geology*, **35**, 787–790, doi: http://dx.doi.org/10.1130/G23637A.1

DEVINE, J., RUTHERFORD, M., NORTON, G. & YOUNG, S. 2003. Magma storage region processes inferred from geochemistry of Fe-Ti oxides in andesitic magma, Soufrière Hills Volcano, Montserrat, W.I. *Journal of Petrology*, **44**, 1375–1400.

DUFEK, J. & BERGANTZ, W. 2005. Lower crustal magma genesis and preservation: a stochastic framework for the evaluation of basalt-crust interaction. *Journal of Petrology*, **46**, 2167–2195.

EILER, J. M. 2001. Oxygen isotope variations of basaltic lavas and upper mantle rocks. *In*: VALLEY, J. W. & COLE, D. R. (eds) *Stable Isotope Geochemistry*. Mineralogical Society of America, Washington, DC, Reviews in Mineralogy series, **43**, 319–364.

ESCOBAR-WOLF, R., MATIAS-GOMEZ, O. & ROSE, W. 2008. Updated geologic map of the Santiaguito dome complex, Guatemala. Abstract presented at the IAVCEI 2008 General Assembly in Reykjavik, Iceland.

ESCOBAR-WOLF, R. P., DIEHL, J. F., SINGER, B. S. & ROSE, W. I. 2010. $^{40}Ar/^{39}Ar$ and paleomagnetic constraints on the evolution of Volcan Santa María, Guatemala. *Geological Society of America Bulletin*, **122**, 757–771.

EVANS, B. & SCAILLET, B. 1997. The redox state of Pinatubo dacite and the ilmenite–hematite solvus. *American Mineralogist*, **82**, 625–629.

GELDMACHER, J., HOERNLE, K., VAN DEN BOGAARD, P., HAUFF, F. & KLÜGEL, A. 2008. Age and geochemistry of the Central American forearc basement (DSDP Leg 67 and 84): insights into Mesozoic arc volcanism and seamount accretion on the fringe of the Caribbean LIP. *Journal of Petrology*, **49**, 1781–1815.

GINIBRE, C., KRONZ, A. & WÖRNER, G. 2002. High-resolution quantitative imaging of plagioclase composition using accumulated backscattered electron images: new constraints on oscillatory zoning. *Contributions to Mineralogy and Petrology*, **142**, 436–448.

GHIORSO, M. & SACK, R. 1991. Fe–Ti oxide geothermometry: thermodynamic formulation and the estimation of intensive variables in silicic magmas. *Contributions to Mineralogy and Petrology*, **119**, 224–238.

HALSOR, S. P. & ROSE, W. I. 1988. Common characteristics of paired volcanoes in northern Central America. *Journal of Geophysical Research*, **93**, 4467–4476.

HARRIS, A. J. L., ROSE, W. I. & FLYNN, L. P. 2003. Temporal trends in lava dome extrusion at Santiaguito 1922–2000. *Bulletin of Volcanology*, **65**, 77–89.

HATTORI, K. 1993. High-sulfur magma, a product of fluid discharge from underlying mafic magma: evidence from Mount Pinatubo, Philippines. *Geology*, **21**, 1083–1086.

HAWKESWORTH, C. J., BLAKE, S. *ET AL.* 2000. Time scales of crystal fractionation in magma chambers – integrating physical, isotopic and geochemical perspectives. *Journal of Petrology*, **41**, 991–1006.

HEYDOLPH, K., HOERNLE, K., HAUFF, F., VAN DEN BOGAARD, P., PORTNYAGIN, M., BINDEMAN, I. & GARBE-SCHONBERG, D. 2012. Along and across arc geochemical variations in NW Central America:

evidence for involvement of lithospheric pyroxenite. *Geochimica et Cosmochimica Acta*, **84**, 459–491.

HILDRETH, W. 1983. The compositionally zoned eruption of 1912 in the Valley of Ten Thousand Smokes, Katmai National Park, Alaska. *Journal of Volcanology and Geothermal Research*, **18**, 1–56.

HILDRETH, W. & MOORBATH, S. 1988. Crustal contributions to arc magmatism in the Andes of central Chile. *Contributions to Mineralogy and Petrology*, **98**, 455–489.

HOFMANN, A. W. & HART, S. M. 1978. An assessment of local and regional isotopic equilibrium in the mantle. *Earth and Planetary Science Letters*, **38**, 44–62.

HORA, J. M., SINGER, B. S. & WORNER, G. 2007. Eruptive flux through thick crust of the Andean central volcanic zone: $^{40}Ar/^{39}Ar$ constraints from Volcán Parinacota, Chile. *Geological Society of America Bulletin*, **119**, 343–362.

HORA, J. M., SINGER, B. S., WORNER, G., BEARD, B. L., JICHA, B. R. & JOHNSON, C. L. 2009. Shallow and deep control on differentiation of calc-alkaline and tholeiitic magma. *Earth and Planetary Science Letters*, **285**, 75–86.

HUMPHREYS, M., BLUNDY, J. & SPARKS, R. 2006. Magma evolution and open-system processes at Shiveluch Volcano: insights from phenocryst zoning. *Journal of Petrology*, **47**, 2303–2334.

JICHA, B. R. & SINGER, B. S. 2006. Volcanic history and magmatic evolution of Seguam Island, Aleutian Island arc, Alaska. *Geological Society of America Bulletin*, **118**, 805–822.

JICHA, B. R., SINGER, B. S., BEARD, B. L. & JOHNSON, C. L. 2005. Contrasting timescales of crystallization and magma storage beneath the Aleutian Island arc. *Earth and Planetary Science Letters*, **236**, 195–210.

JICHA, B. R., SINGER, B. S., BEARD, B. L., JOHNSON, C. L., MORENO-ROA, H. & NARANJO, J. A. 2007. Rapid magma ascent and generation of ^{230}Th excesses in the lower crust at Puyehue-Cordón Caulle, Southern Volcanic Zone, Chile. *Earth and Planetary Science Letters*, **255**, 249–242.

JICHA, B. R., JOHNSON, C. M., HILDRETH, W., BEARD, B. L., HART, G. L., SHIREY, S. B. & SINGER, B. S. 2009. Discriminating assimilants and decoupling deep- vs. shallow-level crystal records at Mount Adams using $^{238}U–^{230}Th$ disequilibria and Os isotopes. *Earth and Planetary Science Letters*, **277**, 38–49.

JICHA, B. R., SMITH, K. E., SINGER, B. S., BEARD, B. L. & JOHNSON, C. M. 2010. Crustal assimilation no match for slab-fluids beneath Volcán de Santa María, Guatemala. *Geology*, **38**, 859–862.

JICHA, B. R., COOMBS, M. L., CALVERT, A. T. & SINGER, B. S. 2012. Geology and $^{40}Ar/^{39}Ar$ geochronology of the medium- to high-K Tanaga volcanic cluster, western Aleutians. *Geological Society of America Bulletin*, **124**, 842–856.

KITA, N., IKEDA, Y., TOGASHI, S., LIU, Y., MORISHITA, Y. & WEISBERG, M. 2004. Origin of ureilites inferred from a SIMS oxygen isotopic and trace element study of clasts in the Dar al Gani 319 polymict ureilite. *Geochimica et Cosmochimica Acta*, **68**, 4213–4235.

MATSUHISA, Y. 1979. Oxygen isotope compositions of volcanic rocks from the east Japan island arcs and their bearing on petrogenesis. *Journal of Volcanology and Geothermal Research*, **5**, 271–296.

MORGAN, G. & LONDON, D. 1996. Optimizing the electron microprobe analysis of hydrous alkali aluminosilicate glasses. *American Mineralogist*, **81**, 1176–1185.

NAKADA, S. & MOTOMURA, Y. 1999. Petrology of the 1991–1995 eruption at Unzen: effusion pulsation and groundmass crystallization. *Journal of Volcanology and Geothermal Research*, **89**, 173–196.

NEWMAN, S. & LOWENSTERN, J. 2002. VolatileCalc: a silicate melt–H_2O–CO_2 solution model written in Visual Basic for excel. *Computers and Geosciences*, **28**, 597–604.

PALLISTER, J., HOBLITT, R. & REYES, A. 1992. A basalt trigger for the 1991 eruptions of Pinatubo volcano? *Nature*, **356**, 426–428.

PATINO, L. C., CARR, M. J. & FEIGENSON, M. D. 2000. Local and regional variations in Central American arc lavas controlled by variations in subducted sediment input. *Contributions to Mineralogy and Petrology*, **138**, 265–283.

PICHAVANT, M., MARTEL, C., BOURDIER, J. & SCAILLET, B. 2002. Physical conditions, structure, and dynamics or a zoned magma chamber: Mount Pelée (Martinique, Lesser Antilles Arc). *Journal of Geophysical Research*, **107**, B5, doi: http://dx.doi.org/10.1029/2001JB000315

PUTIRKA, K. 2008. Thermometers and barometers for volcanic systems. *In*: PUTIRKA, K. & TEPLEY, F. (eds) *Minerals, Inclusions and Volcanic Processes*. Mineralogical Society of America, Washington, DC, Reviews in Mineralogy and Geochemistry, **69**, 61–120.

ROGERS, N., THOMAS, L., MACDONALD, R., HAWKESWORTH, C. & MOKADEM, F. 2006. $^{238}U–^{230}Th$ disequilibrium in recent basalts and dynamic melting beneath the Kenya rift. *Chemical Geology*, **234**, 148–168.

ROMAN, D., CASHMAN, K., GARDNER, C., WALLACE, P. & DONOVAN, J. 2006. Storage and interaction of compositionally heterogeneous magmas from the 1986 eruption of Augustine Volcano, Alaska. *Bulletin of Volcanology*, **68**, 240–254.

ROSE, W. I. 1972. Santiaguito Volcanic Dome, Guatemala. *Geological Society of America Bulletin*, **83**, 1413–1434.

ROSE, W. I. 1987*a*. Santa María, Guatemala: a bimodal soda-rich calc-alkalic Stratovolcano. *Journal of Volcanology and Geothermal Research*, **33**, 109–129.

ROSE, W. I. 1987*b*. Volcanic activity at Santiaguito volcano, 1976–1984. *In*: FINK, J. H. (ed.) *The Emplacement of Silicic Domes and Lava Flows*, Geological Society of America Special Papers, **212**, 17–27.

ROSE, W. I., GRANT, N. K., HAHN, G. A., LANGE, I. M., POWELL, J. L., EASTER, J. & DEGRAFF, J. M. 1977. The evolution of Santa María Volcano, Guatemala. *Geology*, **85**, 63–87.

SAITO, G., KAZAHAYA, K., SHINOHARA, H., STIMAC, J. & KAWANABE, Y. 2001. Variation of volatile concentration in a magma system of Satsuma-Iwojima volcano deduced from melt inclusions analyses. *Journal of Volcanology and Geothermal Research*, **108**, 11–31.

SIMS, K. W. W., GILL, J. B. *ET AL*. 2008. An inter-laboratory assessment of the thorium isotopic composition of synthetic and rock reference materials. *Geostandards and Geoanalytical Research*, **32**, 65–91.

SINGER, B. S., O'NEIL, J. R. & BROPHY, J. G. 1992. Oxygen isotope constraints on the petrogenesis of Aleutian arc magmas. *Geology*, **20**, 367–370.

SINGER, B., DUNGAN, M. & LAYNE, G. 1995. Textures and Sr, Ba, Mg, Fe, K, and Ti compositional profiles in volcanic plagioclase: clues to dynamics of calc-alkaline magma chambers. *American Mineralogist*, **80**, 776–798.

SINGER, B. S., SMITH, K. E., JICHA, B. R., BEARD, B. L., JOHNSON, C. M. & ROGERS, N. W. 2011. Tracking open-system differentiation during growth of Santa María volcano, Guatemala. *Journal of Petrology*, **52**, 2335–2363.

SNYDER, D. 2000. Thermal effects of the intrusion of basaltic magma into a more silicic magma chamber and implications for eruption triggering. *Earth and Planetary Science Letters*, **175**, 257–273.

SPARKS, R. S. J. & MARSHALL, L. A. 1986. Thermal and mechanical constraints on mixing between mafic and silicic magmas. *Journal of Volcanology and Geothermal Research*, **29**, 99–124.

SPARKS, R. S. J., SIGURDSSON, H. & WILSON, L. 1977. Magma mixing: a mechanism for triggering acid explosive eruptions. *Nature*, **267**, 315–318.

SPERA, F. J. & BOHRSON, W. A. 2004. Open-system magma chamber evolution: an energy-constrained geochemical model incorporating the effects of concurrent eruption, recharge, variable assimilation and fractional crystallization (EC-RA$_x$FC). *Journal of Petrology*, **45**, 2459–2480.

SPICUZZA, M. J., VALLEY, J. W. & MCCONNELL, V. S. 1998. Oxygen isotope analysis of whole rock via laser fluorination: an air-lock approach. *Geological Society of America Abstracts with Program*, **30**, 80.

SUN, S. S. & MCDONOUGH, W. F. 1989. Chemical and isotopic systematics of oceanic basalts: implications for mantle composition and processes. *In*: SAUDERS, A. D. & NORRY, M. J. (eds) *Magmatism in the Ocean Basins*. Geological Society, London, Special Publications, **42**, 313–345.

TENNER, T. J., HIRSCHMANN, M. M., WITHERS, A. C. & HERVIG, R. L. 2010. Hydrogen partitioning between nominally anhydrous upper mantle minerals and melt between 3 and 5 GPa and applications to hydrous peridotite melting. *Chemical Geology*, **262**, 42–56.

TRIEBOLD, S., WÖRNER, G. & KRONZ, A. 2006. Anorthite- and celsian-calibrated backscattered electron profiles, trace elements, and growth textures in feldspars from the Teide-Pico Viejo volcano complex (Tenerife). *Journal of Volcanology and Geothermal Research*, **154**, 117–130.

VALLEY, J. W., KITCHEN, N., KOHN, M. J., NIENDORF, C. R. & SPICUZZA, M. J. 1995. UWG-2, a garnet standard for oxygen isotope ratios: strategies for high precision and accuracy with laser heating. *Geochimica et Cosmochimica Acta*, **59**, 5223–5231.

VENEZKY, D. & RUTHERFORD, M. 1999. Petrology and Fe–Ti oxide reequilibration of the 1991 Mount Unzen mixed magma. *Journal of Volcanology and Geothermal Research*, **89**, 213–230.

VOGEL, T. A., PATINO, L. C., EATON, J. K., VALLEY, J. V., ROSE, W. I., ALVARADO, G. E. & VIRAY, E. L. 2006. Origin of silicic magmas along the Central American volcanic front: genetic relationship to mafic melts. *Journal of Volcanology and Geothermal Research*, **156**, 217–228.

WALKER, J. A., CARR, M. J., PATINO, L. C., JOHNSON, C. M., FEIGENSON, M. D. & WARD, R. L. 1995. Abrupt change in magma generation processes across the Central American arc in southeastern Guatemala: flux dominated melting near the base of the wedge to decompression melting near the top of the wedge. *Contributions to Mineralogy and Petrology*, **120**, 378–390.

WALKER, J. A., MICKELSON, J. E. *ET AL.* 2007. U-series disequilibria in Guatemalan lavas, crustal contamination and implications for magma genesis along the Central American subduction zone. *Journal of Geophysical Research*, **112**, 2006JB004589.

WALLACE, P. & GERLACH, T. 1994. Magmatic vapor source for sulfur dioxide released during volcanic eruptions: evidence from Mount Pinatubo. *Science*, **265**, 497–499.

WILLIAMS, S. & SELF, S. 1982. The October 1902 Plinian eruption of Santa María Volcano, Guatemala. *Journal of Volcanology and Geothermal Research*, **16**, 33–56.

WITHAM, C. S. 2005. Volcanic disasters and incidents: a new database. *Journal of Volcanology and Geothermal Research*, **148**, 191–233.